INTERNATIONAL JOURNAL FOR NUMERICAL AND ANALYTICAL METHODS IN GEOMECHANICS, VOL. 22, 197–227 (1998)

ELASTOPLASTIC CONSTITUTIVE EQUATION OF SOILS WITH THE SUBLOADING SURFACE AND THE ROTATIONAL HARDENING

K. HASHIGUCHI AND Z.-P. CHEN

Department of Agricultural Engineering, Kyushu University, Hakozaki, Higashi-ku, Fukuoka-812, Japan

SUMMARY

The subloading surface model fulfills the mechanical requirements for constitutive equations, i.e. the continuity condition, the smoothness condition and the work rate stiffness relaxation and describes pertinently the Masing effect. The constitutive equation of soils is formulated by introducing the subloading surface model and formulating the evolutional rule of rotational hardening for the description of anisotropy. The applicability of the constitutive equation to the prediction of real soil deformation behaviour is verified by predicting monotonic and cyclic loading behaviour of sands under drained and undrained conditions and comparing them with test data. © 1998 John Wiley & Sons, Ltd.

Int. J. Numer. Anal. Meth. Geomech., Vol. 22, 197–227 (1998)

Key words: elastoplasticity; constitutive equation; subloading surface model; cyclic plasticity; soil; rotational hardening

1. INTRODUCTION

The conventional theory of plasticity premises that the interior of the yield surface is an elastic domain. Thus, it is unable to predict a cyclic loading behaviour realistically. Therefore, various cyclic plasticity models to describe a plastic deformation due to a stress change within the yield surface have been proposed in the last three decades. Among them the multi,[1, 2] the two,[3, 4] the single,[5] the infinite,[6] the initial subloading[7, 8] and the (extended) subloading[9] surface models are well-known. The non-linear kinematic hardening model[10, 11] has the same properties as the infinite surface model as has been revealed by some workers.[12–14] The multi, the two, the single and the infinite surface models are regarded as extension of the kinematic hardening model. That is, they premise on the *translation* (parallel movement) of single or multi-yield or loading surface(s). On the other hand, the initial or extended subloading surface model is a novel model which premises on the *expansion/contraction* of *subloading surface* on which a current stress always exists even in an unloading process, while the subloading surface keeps a similarity to the conventional yield surface, renamed the *normal-yield surface*, with respect to the point which is

* Correspondence to: K. Hashiguchi, Department of Agricultural Engineering, Kyushu University Hakozaki, Higashi-ku, Fukuoka-812, Japan.

CCC 363–9061/97/030197–31$17.50
© 1998 John Wiley & Sons, Ltd.
Received 4 June 1996
Revised 11 July 1997

fixed (in the initial one) or moves with a plastic deformation (in the extended one). The bounding surface model with radial mapping[15] proposed in 1980 is regarded to fall within the framework of the initial subloading surface model[7] proposed before then in 1977 from the viewpoint of their basic structures,[16] while the plastic modulus in the former is not formulated pertinently by a consistency condition but is done by an interpolation method in the easygoing way up to present. However, the initial subloading surface model and thus the bounding surface model with radial mapping also are inapplicable to the prediction of cyclic loading behaviour, since the *similarity-centre* (projection-centre) of the normal-yield (bounding) and the subloading surfaces is fixed in these models. For instance, an excessive strain accumulation with open hysteresis loops is predicted for stress amplitudes in entirely positive or entirely negative one side. Then, the initial subloading surface model was improved in such a way that the similarity-centre moves with a plastic deformation and was renamed the extended subloading surface model,[9] hereinafter simply called the *subloading surface model*.

It was clarified by Hashiguchi[17, 18] that among the existing plasticity models the subloading surface model fulfills the fundamental requirements for constitutive equations of materials, i.e. the *continuity condition*, the *smoothness condition* and the *work rate-stiffness relaxation*, obeying the associated flow rule, and describes pertinently the *Masing effect* which is required to predict cyclic loading behaviour. The applicability of this model to metals has been verified[19] and its application to soils has been studied.[20, 21]

The induced anisotropy of metals has been conveniently described by the kinematic hardening, i.e. the translation of yield surface. However, the translation of yield surface cannot be allowed for soils since the yield surface of soils would always have to include the origin of stress space slightly. Therefore, the kinematic hardening may not be applied to soils. On the other hand, Sekiguchi and Ohta[22] proposed a simple description of an inherent anisotropy of K_o consolidated soils by assuming a yield surface rotated around the origin of stress space. Hashiguchi[23, 24] called it a *rotational hardening* and studied its evolutional rule.

In this article, elastoplastic constitutive equation of soils ranging from clays to sands is formulated by incorporating the concept of the subloading surface and formulating the evolutional rule of the rotational hardening for the description of inherent and induced anisotropy. Its adequacy is examined by predicting monotonic and cyclic loading behaviour of sands under drained and undrained conditions and comparing them with experimental data. The signs of a stress (rate) and a stretching (a symmetric part of velocity gradient) are positive for tension, and the stress stands for the effective stress, i.e. the stress excluded a pore pressure from a total stress throughout this article.

2. SUBLOADING SURFACE MODEL WITH ROTATIONAL HARDENING

The subloading surface model[9] premises on the existence of the *subloading surface* which expands/contracts existing inside the yield surface in the conventional sense, renamed the *normal-yield surface* in order to express its physical meaning clearly, passing always through a current stress point in not only a loading but also an unloading process and keeping a similarity to the normal-yield surface. Besides, it is assumed that the subloading surface approaches asymptotically to the normal-yield surface in a loading process, causing a decrease of plastic modulus. In what follows, let the subloading surface model be formulated concretely for soils incorporating the rotational hardening, i.e. the rotation of the normal-yield surface around the origin of stress space.

 © 1998 John Wiley & Sons, Ltd.

The stretching $\mathbf{D}$ (symmetric part of velocity gradient) is additively decomposed into the elastic stretching $\mathbf{D}^{\mathrm{e}}$ and the plastic stretching $\mathbf{D}^{\mathrm{p}}$ as usual, i.e.

$$\mathbf{D} = \mathbf{D}^{\mathrm{e}} + \mathbf{D}^{\mathrm{p}} \tag{1}$$

where the elastic stretching is given by

$$\mathbf{D}^{\mathrm{e}} = \mathbf{E}^{-1}\mathring{\boldsymbol{\sigma}} \tag{2}$$

$\boldsymbol{\sigma}$ is a stress and $(\mathring{})$ indicates the corotational rate. The fourth-order tensor $\mathbf{E}$ is the elastic modulus given in the Hooke's type as

$$E_{ijkl} = \left(K - \frac{2}{3}G\right)\delta_{ij}\delta_{kl} + G(\delta_{ik}\delta_{jl} + \delta_{il}\delta_{jk}) \tag{3}$$

where K and G are the bulk modulus and the shear modulus, respectively, which are functions of stress and internal state variables in general and δ_{ij} is the Kronecker's delta, i.e. $\delta_{ij} = 1$ for $i = j$ and $\delta_{ij} = 0$ *for* $i \neq j$.

Let the normal-yield surface which passes through the origin of stress space and obeys isotropic and rotational hardening be described as

$$f(\hat{p}, \hat{\chi}) = F(H) \tag{4}$$

where, letting the stress on the normal-yield surface be denoted as $\hat{\boldsymbol{\sigma}}$,

$$\hat{\sigma}_m \equiv \tfrac{1}{3}\operatorname{tr}\hat{\boldsymbol{\sigma}}, \quad \hat{p} \equiv -\hat{\sigma}_m, \quad \hat{\boldsymbol{\sigma}}^* \equiv \hat{\boldsymbol{\sigma}} + \hat{p}\mathbf{I} \tag{5}$$

$$\hat{\boldsymbol{\eta}} \equiv \hat{\mathbf{Q}} - \boldsymbol{\beta}, \quad \hat{\mathbf{Q}} \equiv \frac{\hat{\boldsymbol{\sigma}}^*}{\hat{p}} \tag{6}$$

$$\hat{\chi} \equiv \frac{\|\hat{\boldsymbol{\eta}}\|}{\hat{m}} \tag{7}$$

$\hat{m}$ is a function of

$$\sin 3\hat{\theta}_\sigma \equiv -\sqrt{6}\,\frac{\operatorname{tr}\hat{\boldsymbol{\eta}}^3}{\|\hat{\boldsymbol{\eta}}\|^3} \tag{8}$$

including the material constant ϕ, i.e.

$$\hat{m} = f_m(\sin 3\hat{\theta}_\sigma;\, \phi) \tag{9}$$

$\|\ \|$ denoting a magnitude. H is the isotropic hardening variable. The central axis of the normal-yield surface is described as $\boldsymbol{\sigma}^*/p = \boldsymbol{\beta}$, while equation (4) for the normal-yield surface includes only $\boldsymbol{\beta}$ as a variable to describe the anisotropy, where

$$\sigma_m \equiv \tfrac{1}{3}\operatorname{tr}\boldsymbol{\sigma}, \qquad p \equiv -\sigma_m, \quad \boldsymbol{\sigma}^* \equiv \boldsymbol{\sigma} + p\mathbf{I} \tag{10}$$

Let $\boldsymbol{\beta}$ be called the *rotational hardening variable*. The equation $\|\hat{\boldsymbol{\eta}}\| = \hat{m}$ describes a conical surface whose tip exists at the origin and central axis coincides with the central axis $\boldsymbol{\sigma}^*/p = \boldsymbol{\beta}$ of the normal-yield surface, the radius varying with the variable $\hat{\theta}_\sigma$ in the principal stress space.

Hereinafter, it is assumed that the normal-yield surface keeps a similarity to itself. Then, f is a homogeneous function of $\hat{\boldsymbol{\sigma}}$, satisfying Euler's theorem for a homogeneous function. Therefore,

© 1998 John Wiley & Sons, Ltd.

by selecting the function f to be homogeneous degree one, the following expression holds, while $\hat{\chi}$ is a dimensionless variable:

$$f(\hat{p}, \hat{\chi}) = \hat{p} g(\hat{\chi}) \tag{11}$$

The parameter $\hat{\boldsymbol{\eta}}$ was introduced by Sekiguchi and Ohta[22] in order to describe the rotation of yield surface concisely.

For the formulation of the evolutional equation of the rotational hardening variable $\boldsymbol{\beta}$, assume as follows:

(1) The yield surface rotates around the origin of stress space.
(2) There exits a limit in the range of the rotation of the normal-yield surface, and let the surface describing the limit be called the *limit surface for rotational hardening* or the *rotational limit surface*. And let this surface be given by the following conical surface whose tip exists at the origin and central axis coincides with the hydrostatic axis in the principal stress space.

$$\frac{\|\boldsymbol{\sigma}^*\|}{p} = \hat{m}_b \tag{12}$$

where $\hat{m}_b$ is given by the function f_m for $\hat{m}$ of equation (9), the material constant ϕ being replaced by the material constant ϕ_b, i.e.

$$\hat{m}_b = f_m(\sin 3\hat{\theta}_\sigma;\ \phi_b) \tag{13}$$

(3) The central axis of yield surface rotates so as to approach the conjugate line on the rotational limit surface. The angle contained by the plane a ($\operatorname{tr}\boldsymbol{\sigma}^{*3}/\|\boldsymbol{\sigma}^*\|^3 = \operatorname{tr}\boldsymbol{\beta}^3/\|\boldsymbol{\beta}\|^3$) including the hydrostatic axis ($\boldsymbol{\sigma}^*/p = \mathbf{O}$) and the central axis ($\boldsymbol{\sigma}^*/p = \boldsymbol{\beta}$) of the yield surface and the plane b ($\operatorname{tr}\boldsymbol{\sigma}^{*3}/\|\boldsymbol{\sigma}^*\|^3 = \operatorname{tr}\hat{\boldsymbol{\eta}}^3/\|\hat{\boldsymbol{\eta}}\|^3$) including the central axis of yield surface and the current stress point is identical to the angle contained by the plane a and the plane c ($\operatorname{tr}(\boldsymbol{\sigma}^*/p - \boldsymbol{\beta})^3/\|\boldsymbol{\sigma}^*/p - \boldsymbol{\beta}\|^3 = \operatorname{tr}\hat{\boldsymbol{\eta}}^3/\|\hat{\boldsymbol{\eta}}\|^3$) including the hydrostatic axis and the conjugate line (see Figure 1). Thus, the conjugate line is given by the equation $\boldsymbol{\sigma}^*/p = \hat{m}_b\hat{\boldsymbol{\eta}}/\|\hat{\boldsymbol{\eta}}\|$.
(4) For monotonic-proportional loading with $\hat{\mathbf{Q}} = \text{const.}$, i.e. the so-called anisotropic consolidation, the central axis of yield surface approaches the loading path, so as to satisfy $\|\hat{\boldsymbol{\eta}}\| = 0$.
(5) The rotational rate of the normal-yield surface is proportional to the magnitude of plastic deviatoric stretching, while it is independent of plastic volumetric stretching which would not be related to anisotropy.

Then, let the evolutional rule of $\boldsymbol{\beta}$ be assumed as

$$\mathring{\boldsymbol{\beta}} = b_r \|\mathbf{D}^{p*}\| \|\hat{\boldsymbol{\eta}}\| \hat{\boldsymbol{\eta}}_b \tag{14}$$

where b_r is the material constant and

$$D_v^p \equiv \operatorname{tr}\mathbf{D}^p, \quad \mathbf{D}^{p*} \equiv \mathbf{D}^p - \tfrac{1}{3} D_v^p \mathbf{I} \tag{15}$$

$$\hat{\boldsymbol{\eta}}_b \equiv \hat{m}_b \hat{t} - \boldsymbol{\beta} \tag{16}$$

$$\hat{t} \equiv \frac{\hat{\boldsymbol{\eta}}}{\|\hat{\boldsymbol{\eta}}\|} \tag{17}$$

In what follows, let the subloading surface concept be introduced.

 © 1998 John Wiley & Sons, Ltd.

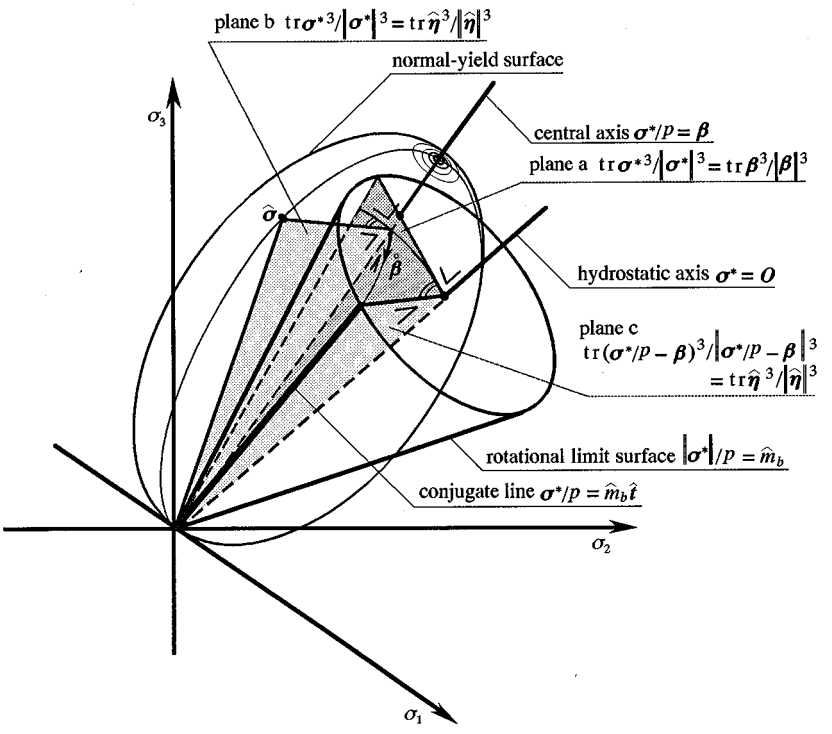

Figure 1. Rotational hardening illustrated in the principal stress space

The subloading surface is given by the similarity to the normal-yield surface (4) as

$$f(\bar{p}, \bar{\chi}) = RF(H) \tag{18}$$

where

$$\bar{\boldsymbol{\sigma}} \equiv \boldsymbol{\sigma} - \bar{\boldsymbol{\alpha}} \tag{19}$$

$$\bar{p} \equiv -\tfrac{1}{3}\,\mathrm{tr}\,\bar{\boldsymbol{\sigma}}, \qquad \bar{\boldsymbol{\sigma}}^* \equiv \bar{\boldsymbol{\sigma}} + \bar{p}\mathbf{I} \tag{20}$$

$$\bar{\boldsymbol{\eta}} \equiv \bar{\mathbf{Q}} - \boldsymbol{\beta}, \quad \bar{\mathbf{Q}} \equiv \frac{\bar{\boldsymbol{\sigma}}^*}{\bar{p}} \tag{21}$$

$$\bar{\chi} \equiv \frac{\|\bar{\boldsymbol{\eta}}\|}{\bar{m}} \tag{22}$$

$\bar{m}$ is a function f_m of

$$\sin 3\bar{\theta}_\sigma \equiv -\sqrt{6}\,\frac{\mathrm{tr}\,\bar{\boldsymbol{\eta}}^3}{\|\bar{\boldsymbol{\eta}}\|^3} \tag{23}$$

including the material constant ϕ, i.e.

$$\bar{m} = f_m(\sin 3\bar{\theta}_\sigma;\ \phi) \tag{24}$$

© 1998 John Wiley & Sons, Ltd.

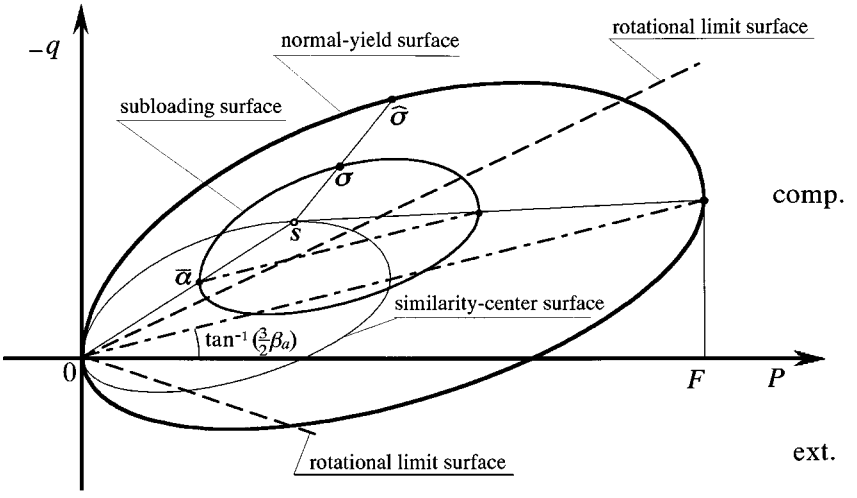

Figure 2. Normal-yield and subloading surfaces with a rotational hardening illustrated for the axisymmetric stress state in the (p, q) space

Needless to say, $\boldsymbol{\sigma}$ stands for a current stress which exits always on the subloading surface. $\bar{\boldsymbol{\alpha}}$ on the subloading surface is the conjugate point of the null stress on the normal-yield surface as is illustrated for the axisymmetric stress state in Figure 2. R $(0 \leqslant R \leqslant 1)$ is the ratio of the size of the subloading surface to that of the normal-yield surface, while $R = 0$ and 1 correspond to the purely elastic and the normal-yield state, respectively. The similarity of the normal-yield and the subloading surfaces leads to the relations

$$\begin{gathered} \bar{\boldsymbol{\sigma}} = R\hat{\boldsymbol{\sigma}}, \qquad \bar{\mathbf{s}} = \mathbf{R}\mathbf{s} \\ \bar{\mathbf{Q}} = \hat{\mathbf{Q}}, \quad \bar{\boldsymbol{\eta}} = \hat{\boldsymbol{\eta}}, \quad \bar{\theta}_\sigma = \hat{\theta}_\sigma, \quad \bar{m} = \hat{m}, \quad \bar{\mathrm{m}}_b = \hat{m}_b, \quad \bar{\chi} = \hat{\chi} \end{gathered} \tag{25}$$

where

$$\bar{\mathbf{s}} \equiv \mathbf{s} - \bar{\boldsymbol{\alpha}} \tag{26}$$

referring to Figure 2 in which β_{a} is the axial component of $\boldsymbol{\beta}$, and

$$q \equiv \sigma_{\mathrm{a}} - \sigma_{\mathrm{l}} \tag{27}$$

σ_{a} and σ_{l} being the axial and the lateral stress, respectively, in the axisymmetric stress state. Hereinafter, let $\hat{\boldsymbol{\sigma}}$ be regarded as the conjugate stress on the normal-yield surface for the current stress on the subloading surface. $\mathbf{s}$ is the *centre of similarity* (or *similarity-centre*) of the normal-yield and the subloading surfaces. Besides, the following expression similar to equation (11) holds:

$$f(\bar{p}, \bar{\chi}) = \bar{p}g(\bar{\chi}) \tag{28}$$

The variable R is calculated from equation (18) with the substitution of

$$\bar{\boldsymbol{\sigma}} = \boldsymbol{\sigma} - (1 - R)\mathbf{s} \tag{29}$$

 © 1998 John Wiley & Sons, Ltd.

obtained from equations (19), $(25)_2$ and (26), and then $\bar{\boldsymbol{\alpha}}$ is calculated by the equation $\bar{\boldsymbol{\alpha}} = (1 - R)\mathbf{s}$.

The evolutional rule of rotational hardening for the general state where the current stress exists on the normal-yield surface or in its interior is given from equations (14)–(17) and (25) as

$$\mathring{\boldsymbol{\beta}} = b_r \|\mathbf{D}^{p*}\| \, \|\bar{\boldsymbol{\eta}}\| \bar{\boldsymbol{\eta}}_b \tag{30}$$

where

$$\bar{\boldsymbol{\eta}}_b = \bar{m}_b \bar{\mathbf{t}} - \boldsymbol{\beta} \tag{31}$$

$$\bar{\mathbf{t}} \equiv \frac{\bar{\boldsymbol{\eta}}}{\|\bar{\boldsymbol{\eta}}\|} \tag{32}$$

$$\bar{m}_b = f_m(\sin 3\bar{\theta}_\sigma;\ \phi_b) \tag{33}$$

Let the evolutional rule of the similarity-centre $\mathbf{s}$ of the normal-yield and the subloading surfaces be formulated below.

The surface which passes through the similarity-centre $\mathbf{s}$ and is similar to the normal-yield surface with respect to the origin of stress space, called the *similarity-centre surface* (see Figure 2), is described as

$$f(p_s, \chi_s) = R_s F(H) \tag{34}$$

where R_s $(0 \leqslant R_s \leqslant 1)$ is the ratio of the size of similarity-centre surface to that of normal-yield surface. The following expression which is similar to equations (11) and (28) holds:

$$f(p_s, \chi_s) = p_s g(\chi_s) \tag{35}$$

where

$$p_s \equiv -\tfrac{1}{3} \operatorname{tr} \mathbf{s}, \qquad \mathbf{s}^* \equiv \mathbf{s} + p_s \mathbf{I} \tag{36}$$

$$\boldsymbol{\eta}_s \equiv \mathbf{Q}_s - \boldsymbol{\beta}, \quad \mathbf{Q}_s \equiv \frac{\mathbf{s}^*}{p_s} \tag{37}$$

$$\chi_s \equiv \frac{\|\boldsymbol{\eta}_s\|}{m_s} \tag{38}$$

m_s is a function f_m of

$$\sin 3\theta_s \equiv -\sqrt{6}\, \frac{\operatorname{tr} \boldsymbol{\eta}_s^3}{\|\boldsymbol{\eta}_s\|^3} \tag{39}$$

including the material constant ϕ, i.e.

$$m_s = f_m(\sin 3\theta_s;\ \phi) \tag{40}$$

The following inequality must hold since the similarity-centre has to exist inside the normal-yield surface, i.e. the similarity-centre surface cannot become larger than the normal-yield surface:

$$f(p_s, \chi_s) \leqslant F(H) \tag{41}$$

© 1998 John Wiley & Sons, Ltd.

Equation (41) leads in the differential form to

$$\mathrm{tr}\left[\frac{\partial f(p_s, \chi_s)}{\partial \mathbf{s}}\left(\mathring{\mathbf{s}} + \frac{1}{F}\left\{\mathrm{tr}\left(\frac{\partial f(p_s, \chi_s)}{\partial \boldsymbol{\beta}}\mathring{\boldsymbol{\beta}}\right) - \dot{F}\right\}\mathbf{s}\right)\right] \leqslant 0 \quad \text{for } f(p_s, \chi_s) = F(H), \text{ i.e. } R_s = 1 \tag{42}$$

where $(\mathring{\ })$ indicates a material-time derivative. Equations (41) or (42) are called the *enclosing condition of similarity-centre*.

In the state $R_s = 1$ in which the similarity-centre exists on the normal-yield surface the vector $\boldsymbol{\sigma} - \mathbf{s}$ makes an obtuse angle with the vector $\partial f(p_s, \chi_s)/\partial \mathbf{s}$ which is outward normal to the similarity-centre surface coinciding with the normal-yield surface, while $\boldsymbol{\sigma}$ exists inside the normal-yield surface. Then, let the following equation be assumed, which satisfies inequality (42):

$$\mathring{\mathbf{s}} + \frac{1}{F}\left\{\mathrm{tr}\left(\frac{\partial f(p_s, \chi_s)}{\partial \boldsymbol{\beta}}\mathring{\boldsymbol{\beta}}\right) - \dot{F}\right\}\mathbf{s} = c\|\mathbf{D}^{\mathrm{p}}\|\tilde{\boldsymbol{\sigma}} \tag{43}$$

from which the evolutional rule of the similarity-centre is obtained as follows:

$$\mathring{\mathbf{s}} = c\|\mathbf{D}^{\mathrm{p}}\|\tilde{\boldsymbol{\sigma}} + \frac{1}{F}\left\{\dot{F} - \mathrm{tr}\left(\frac{\partial f(p_s, \chi_s)}{\partial \boldsymbol{\beta}}\mathring{\boldsymbol{\beta}}\right)\right\}\mathbf{s} \tag{44}$$

where c is a material constant and

$$\tilde{\boldsymbol{\sigma}} \equiv \boldsymbol{\sigma} - \mathbf{s} \tag{45}$$

Differentiation of equation (18) leads to

$$\mathrm{tr}\left\{\frac{\partial f(\bar{p}, \bar{\chi})}{\partial \bar{\boldsymbol{\sigma}}}\mathring{\bar{\boldsymbol{\sigma}}}\right\} + \mathrm{tr}\left\{\frac{\partial f(\bar{p}, \bar{\chi})}{\partial \boldsymbol{\beta}}\mathring{\boldsymbol{\beta}}\right\} = R\dot{F} + \dot{R}F \tag{46}$$

where $\mathring{\bar{\boldsymbol{\sigma}}}$ is given from equation (29) as

$$\mathring{\bar{\boldsymbol{\sigma}}} = \mathring{\boldsymbol{\sigma}} - (1 - R)\mathring{\mathbf{s}} + \dot{R}\mathbf{s} \tag{47}$$

Equation (46) includes $\dot{R}$ in addition to the stress rate $\mathring{\boldsymbol{\sigma}}$ and rates of internal state variables $\dot{F}$, $\mathring{\boldsymbol{\beta}}$, $\mathring{\mathbf{s}}$ which are related to the plastic stretching $\mathbf{D}^{\mathrm{p}}$. Therefore, the relation of $\dot{R}$ to $\mathbf{D}^{\mathrm{p}}$ has to be formulated in order to use equation (46) as a consistency condition.

Then, assume that the stress and thus the subloading surface approaches the normal-yield surface, i.e. that the ratio R of the size of the subloading surface to that of the normal-yield surface increases monotonically satisfying the following relation in the plastic loading process:

$$\left.\begin{aligned} R = 0: &\quad \dot{R} = +\infty, \\ 0 < R < 1: &\quad \dot{R} > 0, \\ R = 1: &\quad \dot{R} = 0, \\ R > 1: &\quad \dot{R} < 0 \end{aligned}\right\} \quad \text{for } \mathbf{D}^{\mathrm{p}} \neq \mathbf{O} \tag{48}$$

Then, the evolutional rule of R in the plastic loading process is given as

$$\dot{R} = U\|\mathbf{D}^{\mathrm{p}}\| \quad \text{for } \mathbf{D}^{\mathrm{p}} \neq \mathbf{O} \tag{49}$$

 © 1998 John Wiley & Sons, Ltd.

where U is the monotonically decreasing function of R satisfying

$$\begin{aligned} R = 0: &\quad U = +\infty \\ 0 < R < 1: &\quad U > 0 \\ R = 1: &\quad U = 0 \\ R > 1: &\quad U < 0 \end{aligned} \tag{50}$$

Examples of the function U are as follows:

$$U = u_1(1/R^{m_1} - 1) \tag{51a}$$

$$U = -u_2 \ln R \tag{51b}$$

where u_1, u_2 and m_1 are material constants. Note that it is not guaranteed for the stress to approach the normal-yield surface in the plastic loading process unless equation (49) is incorporated into the constitutive equation.

Substituting equation (49) into equation (46), the following extended consistency condition for the subloading surface is obtained:

$$\mathrm{tr}\left\{\frac{\partial f(\bar{p}, \bar{\chi})}{\partial \bar{\boldsymbol{\sigma}}} \mathring{\bar{\boldsymbol{\sigma}}}\right\} + \mathrm{tr}\left\{\frac{\partial f(\bar{p}, \bar{\chi})}{\partial \boldsymbol{\beta}} \mathring{\boldsymbol{\beta}}\right\} = R\dot{F} + U \|\mathbf{D}^{\mathrm{p}}\| F \tag{52}$$

The associated flow rule is adopted:

$$\mathbf{D}^{\mathrm{p}} = \lambda \bar{\mathbf{N}} \quad (\lambda > 0) \tag{53}$$

where λ is the positive proportionality factor, and the second-order tensor $\bar{\mathbf{N}}$ is the normalized outward normal of the subloading surface, i.e.

$$\bar{\mathbf{N}} \equiv \frac{\partial f(\bar{p}, \bar{\chi})}{\partial \boldsymbol{\sigma}} \Bigg/ \left\| \frac{\partial f(\bar{p}, \bar{\chi})}{\partial \boldsymbol{\sigma}} \right\| \tag{54}$$

Substituting equations (30), (47) and (53) into the extended consistency condition (52) for the subloading surface and further the result into equations (1) and (2), the positive proportionality factor λ is obtained as

$$\lambda = \frac{\mathrm{tr}(\bar{\mathbf{N}} \mathring{\boldsymbol{\sigma}})}{D_{\mathrm{p}}} = \frac{\mathrm{tr}(\bar{\mathbf{N}}\mathbf{E}\mathbf{D})}{D_{\mathrm{p}} + \mathrm{tr}(\bar{\mathbf{N}}\mathbf{E}\bar{\mathbf{N}})} \tag{55}$$

where

$$D_{\mathrm{p}} \equiv \mathrm{tr}(\bar{\mathbf{N}}\bar{\mathbf{a}}) + \mathrm{tr}(\bar{\mathbf{N}}\bar{\boldsymbol{\sigma}}) \left\{ \frac{F'}{F} h - \frac{1}{RF} \mathrm{tr}\left(\frac{\partial f(\bar{p}, \bar{\chi})}{\partial \boldsymbol{\beta}} \mathbf{b} \right) + \frac{U}{R} \right\} \tag{56}$$

$$\bar{\mathbf{a}} \equiv \frac{\mathring{\bar{\boldsymbol{\alpha}}}}{\lambda} = (1 - R) z - U \mathbf{s} \tag{57}$$

$$F' \equiv \frac{\mathrm{d}F}{\mathrm{d}H}, \qquad h \equiv \frac{\dot{H}}{\lambda} \quad (\dot{F} = F' \lambda h) \tag{58}$$

© 1998 John Wiley & Sons, Ltd.

$$\mathbf{b} \equiv \frac{\mathring{\bar{\boldsymbol{\beta}}}}{\lambda} = b_r \|\bar{\mathbf{N}}^*\| \|\bar{\boldsymbol{\eta}}\| \bar{\boldsymbol{\eta}}_b \tag{59}$$

$$z \equiv \frac{\mathring{\mathbf{s}}}{\lambda} = c\tilde{\boldsymbol{\sigma}} + \frac{1}{F}\left\{F'h - \mathrm{tr}\left(\frac{\partial f(p_s, \chi_s)}{\partial \boldsymbol{\beta}}\mathbf{b}\right)\right\}\mathbf{s} \tag{60}$$

$$\bar{\mathbf{N}}^* \equiv \bar{\mathbf{N}} - \tfrac{1}{3}(\mathrm{tr}\,\bar{\mathbf{N}})\mathbf{I} \tag{61}$$

The loading criterion[25–27] is given by

$$\left.\begin{aligned} &\mathbf{D}^{\mathrm{p}} \neq \mathbf{O}: \quad \mathrm{tr}(\bar{\mathbf{N}}\mathbf{E}\mathbf{D}) > 0 \\ &\mathbf{D}^{\mathrm{p}} = \mathbf{O}: \quad \mathrm{tr}(\bar{\mathbf{N}}\mathbf{E}\mathbf{D}) \leqslant 0 \end{aligned}\right\} \tag{62}$$

3. MATERIAL FUNCTIONS

Particular forms of the material functions in the present model for soils are given in this section.

Let the following material functions for the subloading surface and the similarity-centre surface be adopted:

$$g(\bar{\chi}) = 1 + \bar{\chi}^2, \; g(\chi_s) = 1 + \chi_s^2 \tag{63}$$

The meridian section of the subloading surface given by equations (18), (28) and $(63)_1$ for $\bar{\theta}_\sigma = \text{const.}$ in the case of $\boldsymbol{\beta} = \mathbf{O}$ is a half-ellipsoid whose long axis is parallel to the hydrostatic axis in the stress space. Further, let the following equations be also assumed:

$$\begin{aligned} \bar{m} &= \frac{2\sqrt{6}\sin\phi}{3\{1 + a(1 - \sin^2 3\bar{\theta}_\sigma)\} - \sin\phi \sin 3\bar{\theta}_\sigma} \\ m_s &= \frac{2\sqrt{6}\sin\phi}{3\{1 + a(1 - \sin^2 3\theta_s)\} - \sin\phi \sin 3\theta_s} \\ \bar{m}_b &= \frac{2\sqrt{6}\sin\phi_b}{3\{1 + a(1 - \sin^2 3\bar{\theta}_\sigma)\} - \sin\phi_b \sin 3\bar{\theta}_\sigma} \end{aligned} \tag{64}$$

The equation $\bar{\chi} = 1$, i.e. $\|\bar{\boldsymbol{\eta}}\| = \bar{m}$ with $\bar{m}$ in equation $(64)_1$ coincides with the Coulomb–Mohr failure criterion in the axisymmetric tension/compression state, i.e. $\|\boldsymbol{\sigma}^*\|/p = 2\sqrt{6}\sin\phi/(3 \pm \sin\phi)$ (+: extension ($\bar{\theta}_\sigma = -\pi/6$), −: compression ($\bar{\theta}_\sigma = \pi/6$)) for $\tilde{\boldsymbol{\alpha}} = \mathbf{O}$ and $\boldsymbol{\beta} = \mathbf{O}$, and fulfills the convexity for $0{\cdot}0493 < a < 0.176$ in the range $0 \leqslant \phi \leqslant 45^\circ$. Hereinafter, a is fixed to be 0.1 for brevity.

On the formulation of the isotropic hardening/softening function $F(H)$ first assume the linear relation between $\ln v$ and $\ln p$[28,29] (v: volume) as shown in Figure 3:

$$\begin{aligned} \varepsilon_v &= \varepsilon_v^{\mathrm{p}} + \varepsilon_v^{\mathrm{e}} \\ &= \ln\frac{v^{\mathrm{p}}}{v_0} + \ln\frac{v}{v^{\mathrm{p}}} \\ &= -(\rho - \gamma)\ln\left(\frac{p_y + p_i}{p_{y0} + p_i}\right) - \gamma\ln\left(\frac{p + p_i}{p_0 + p_i}\right) \end{aligned} \tag{65}$$

 © 1998 John Wiley & Sons, Ltd.

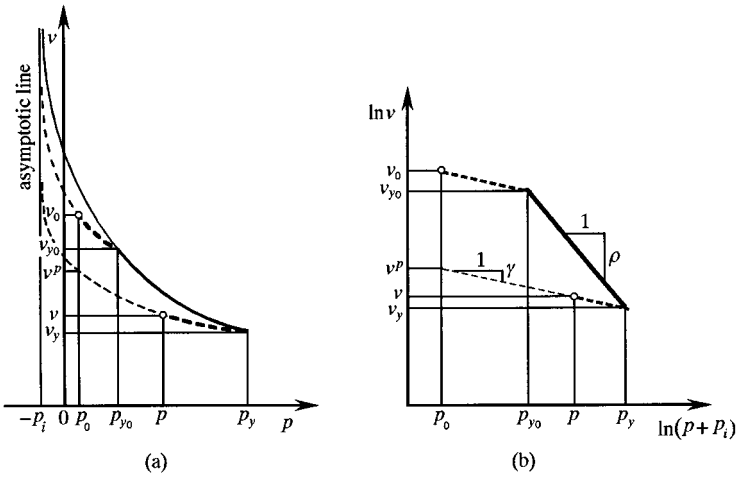

Figure 3. Isotropic consolidation of soils: (a) v–p relation, (b) Idealization as the ln v–ln p linear relation

the time derivative of which is given as

$$D_v = D_v^{\mathrm{p}} + D_v^{\mathrm{e}} = -(\rho - \gamma)\frac{p_y}{p_y + p_i} - \gamma\frac{\dot{p}}{p + p_i} \tag{66}$$

where

$$\begin{aligned} D_v &\equiv \operatorname{tr}\mathbf{D}, \quad \varepsilon_v \equiv \int D_v \,\mathrm{d}t \\ D_v^{\mathrm{e}} &\equiv \operatorname{tr}\mathbf{D}^{\mathrm{e}}, \quad \varepsilon_v^{\mathrm{e}} \equiv \int D_v^{\mathrm{e}} \,\mathrm{d}t \\ D_v^{\mathrm{p}} &\equiv \operatorname{tr}\mathbf{D}^{\mathrm{p}}, \quad \varepsilon_v^{\mathrm{p}} \equiv \int D_v^{\mathrm{p}} \,\mathrm{d}t \end{aligned} \tag{67}$$

ε_v, $\varepsilon_v^{\mathrm{e}}$ and $\varepsilon_v^{\mathrm{p}}$ are volumetric, elastic volumetric and plastic volumetric strain, respectively, in the definition of the logarithmic strain. v_0 is the initial volume and v^{p} is the volume in the unloaded state to the initial pressure p_0, and p_y and p_{y0} are yield pressure and its initial value, respectively. p_i is the material constant, while $-p_i$ is a negative pressure for which a volume becomes infinite, i.e. $v \to \infty$ for $p \to -p_i$. ρ and γ are the material constants describing the slopes of the normal consolidation (elastoplastic) curve and the swelling (elastic) curve, respectively, in the $(\ln p, \ln v)$ space.

By selecting F to be equal to p_y in equation (65), one has

$$F = (F_0 + p_i)\exp\left(\frac{-\varepsilon_v^{\mathrm{p}}}{\rho - \gamma}\right) - p_i \tag{68}$$

for the isotropic consolidation process, where F_0 is the initial value of F. Isotropic hardening/softening of soils is substantially induced by the decrease/increase of plastic volumetric

© 1998 John Wiley & Sons, Ltd.

stretching. The isotropic hardening/softening function for clays is given by equation (68). On the other hand, the isotropic hardening/softening for sands is also induced by a plastic shear deformation. From experimental results[30,31] for the axisymmetric compression/extension under undrained conditions in which a plastic volume change is very small compared to a shear deformation it is known that loose sands deforming at a low stress ratio $\|\boldsymbol{\sigma}^*\|/p$ undergo a remarkable softening reaching a null strength but dense sands deforming at a high stress ratio do a remarkable hardening climbing up along the straight line of the high stress ratio by a plastic shear deformation. Then, assume that the plastic shear deformation causes a softening and a hardening for the stress state inside and outside, respectively, of the surface, called the *shear boundary surface*, forming a conical surface whose tip exists in the origin and central axis coincides with the hydrostatic axis in the principal stress space as shown in the (p, q) space of Figure 4, similar to the rotational limit surface. And let this surface be described as

$$\frac{\|\boldsymbol{\sigma}^*\|}{p} = m_d \tag{69}$$

$$m_d = f_m(\theta_\sigma;\phi_d) = \frac{2\sqrt{6}\sin\phi_d}{3\{1 + a(1 - \sin^2 3\theta_\sigma)\} - \sin\phi_d \sin 3\theta_\sigma} \tag{70}$$

where ϕ_d is the material constant, while the looser the sand is, the larger ϕ_d is, and

$$\sin 3\theta_\sigma \equiv -\sqrt{6}\frac{\operatorname{tr}\boldsymbol{\sigma}^{*3}}{\|\boldsymbol{\sigma}^*\|^3} \tag{71}$$

Then, let the isotropic hardening/softening function be given as

$$F = (F_0 + p_i)\exp\left(\frac{H}{\rho - \gamma}\right) - p_i \tag{72}$$

$$\dot{H} = -D_v^{\mathrm{p}} + D_s^{\mathrm{p}} \tag{73}$$

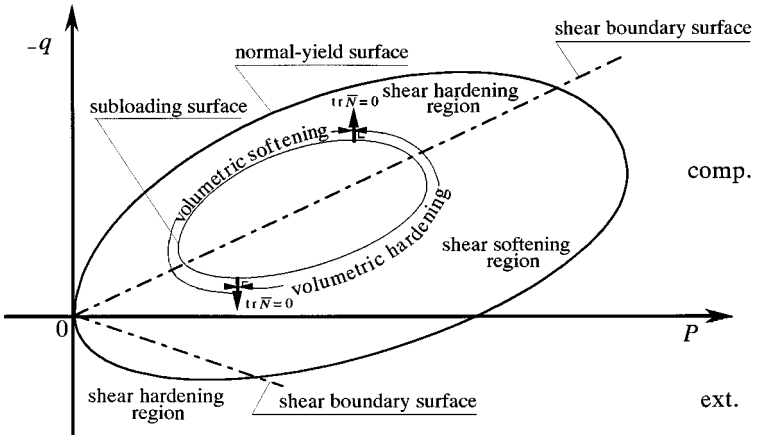

Figure 4. Volumetric and shear hardening/softening regions illustrated for the axisymmetric stress state in the (p, q) space

 © 1998 John Wiley & Sons, Ltd.

where

$$D_s^{\mathrm{p}} \equiv \mu \| \mathbf{D}^{\mathrm{p}*} \| \left(\frac{\| \boldsymbol{\sigma}^* \|}{p} - m_d \right) \tag{74}$$

and μ is a material constant. From equations (72)–(74) it holds for equation (58) that

$$F' = \frac{F + p_i}{\rho - \gamma}, \qquad h = -\operatorname{tr} \bar{\mathbf{N}} + \mu \| \bar{\mathbf{N}}^* \| \left(\frac{\| \boldsymbol{\sigma}^* \|}{p} - m_d \right) \tag{75}$$

Let the elastic bulk modulus K be given from equation (66) as

$$K = \frac{p + p_i}{\gamma} \tag{76}$$

The elastic stretching is given from equation (2) with equations (3) and (76) as

$$\mathbf{D}^{\mathrm{e}} = \frac{1}{3} \frac{\gamma}{p + p_i} \dot{\sigma}_{\mathrm{m}} \mathbf{I} + \frac{1}{2G} \mathring{\boldsymbol{\sigma}}^* \tag{77}$$

4. IDENTIFICATION OF MATERIAL PARAMETERS

The constitutive equation proposed in this article includes 12 material parameters and three internal variables whose initial values have to be determined prior to the calculation.

ρ, γ and p_i are determined from the isotropic normal consolidation and swelling curves. G is determined from the inclination of the unloading curve in triaxial compression test result. μ and ϕ_d are determined from the undrained stress path.

u_1 and m_1 regulate the approaching rate to the normal-yield state. c affects the width of hysteresis loop. b_r and ϕ_b describe the rate and the range, respectively, of the evolution of the anisotropic hardening. They are related to each other in describing the size and the shape of stress paths and stress–strain curves, and thus have to be determined so as to fit the test results by the trial and error method, however.

F_0/p_0 (p_0: initial pressure) corresponds to the overconsolidation ratio in clays. $\boldsymbol{\beta}_0$ is determined by the stress path of anisotropic consolidation. $\mathbf{s}_0$ would have to be determined by the trial and error method at present.

The identification of these parameters, especially their dependence on the relative density, and the initial values of internal variables will require an accumulation of curve-fitting results and a more due consideration on their physical meanings.

5. COMPARISONS WITH EXPERIMENTS

In order to examine the ability of the present model to reproduce the real soil behaviour in an acceptable way, the simulation results in several series of test data for sands on the drained and the undrained conditions are shown in this section.

5.1. Drained tests

The test data of Hostun sand are used as comparisons in the drained condition, which were presented in the "International Workshop on Constitutive Equations for Granular Non-cohesive Soils"[32] held in 1987 in Cleveland, U.S.A.

© 1998 John Wiley & Sons, Ltd.

The Hostun sand used for the tests is a poorly graded material with similar grain size distribution. Tests were done in the dense state with the initial void ratio $e_0 = 0{\cdot}616$ under the initial pressure $p_0 = 100\,\mathrm{kPa}$, using the true triaxial (cubical) test apparatus and the hollow cylinder test apparatus.

The co-ordinate system (x, y, z) for the true triaxial test apparatus is taken as shown in Figure 5 where $\sigma_x, \sigma_y, \sigma_z$ are principal stresses. $\varepsilon_x, \varepsilon_y, \varepsilon_z$ are calculated by the time integration of the three principal stretchings D_x, D_y, D_z. The co-ordinate system (r, θ, z) for the hollow cylinder test apparatus is taken as shown in Figure 6 where σ_r is always a principal stress with $\tau_{r\theta} = \tau_{zr} = 0$.

The following material constants and initial values are used in all calculations and all the calculations are done from the same initial isotropic stress state $\boldsymbol{\sigma}_0 = -100\mathbf{I}\,\mathrm{kPa}$, although initial values shown in the test data are different in each test.

material constants:

yield surface (ellipsoid) shape $\phi = 27^\circ$

$$\text{hardening/softening} \begin{cases} \text{isotropic} \begin{cases} \text{volumetric } \rho = 0{\cdot}008,\ p_i = 10\,\mathrm{kPa} \\ \text{deviatoric } \mu = 0{\cdot}6,\ \phi_d = 25^\circ \end{cases} \\ \text{rotational } b_r = 110,\ \phi_b = 26^\circ \end{cases}.$$

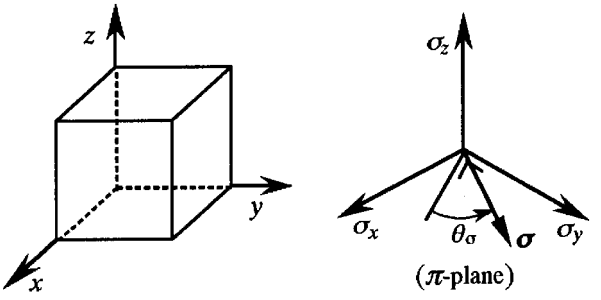

Figure 5. Rectangular co-ordinates (x, y, z) and the variables for the true triaxial test apparatus

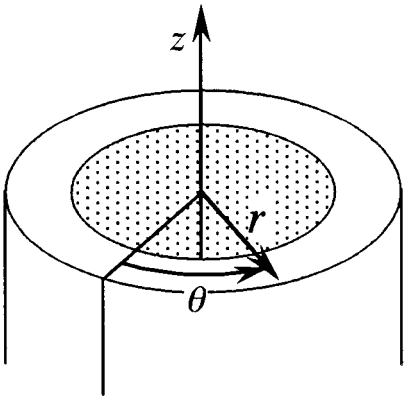

Figure 6. Cylindrical co-ordinates (r, θ, z) for the hollow cylinder test apparatus

 © 1998 John Wiley & Sons, Ltd.

evolution of R $u_1 = 1{\cdot}5$, $m_1 = 3{\cdot}8$
movement of similarity–centre $c = 20$
elastic constants $\gamma = 0{\cdot}003$, $G = 200{,}000\,\mathrm{kPa}$

initial values:

$F_0 = 400\,\mathrm{kPa}$, $\boldsymbol{\beta}_0 = \mathbf{O}$, $\mathbf{s}_0 = -50\mathbf{I}\,\mathrm{kPa}$,
$\boldsymbol{\sigma}_0 = -100\mathbf{I}\,\mathrm{kPa}$

where $\boldsymbol{\beta}_0$, $\mathbf{s}_0$ and $\boldsymbol{\sigma}_0$ are initial values of $\boldsymbol{\beta}$, $\mathbf{s}$ and $\boldsymbol{\sigma}$, respectively.

The test data and the calculated results are depicted by the dashed and the solid curves, respectively.

5.1.1. Cyclic isotropic loading: true triaxial test apparatus. The cyclic isotropic loading $p(=-\sigma_x=-\sigma_y=-\sigma_z) = 100 \to 610 \to 75 \to 1{,}100 \to 70 \to 2{,}145 \to 137\,\mathrm{kPa}$ is shown in Figure 7. Hysteresis loops are simulated well by the movement of similarity-centre, although the compressive strain is predicted to be smaller than the test data in the state that a pressure is greater than 1,000 kPa.

5.1.2. Axisymmetric compression with a constant lateral stress: true triaxial test apparatus. The compression with a constant lateral stress $(-\sigma_x = -\sigma_y = 200\,\mathrm{kPa} \leqslant -\sigma_z)$ from $\boldsymbol{\sigma} = -200\mathbf{I}\,\mathrm{kPa}$ is shown in Figure 8. The relations of the dimensionless stress level $\|\boldsymbol{\sigma}^*\|/(3p)$ and the volumetric strain ε_v vs. the magnitude of deviatoric strain $\|\boldsymbol{\varepsilon}^*\|$ are depicted. The response in unloading and reloading is predicted to be stiffer than the test data and thus the hysteresis loop is predicted to be smaller than that. The volumetric strain is predicted well, while the associated flow rule is adopted. This is caused by the fact that the outward normal of subloading surface at the current stress point can have the negative component of mean stress axis even in state denser than critical state (the overconsolidated state for clays) as will be described in Section 6.

5.1.3. Axisymmetric extension with a constant lateral stress: true triaxial test apparatus. The extension with a constant lateral stress $(-\sigma_x = -\sigma_y = 200\,\mathrm{kPa} \geqslant -\sigma_z)$ from $\boldsymbol{\sigma} = -200\mathbf{I}\,\mathrm{kPa}$ is

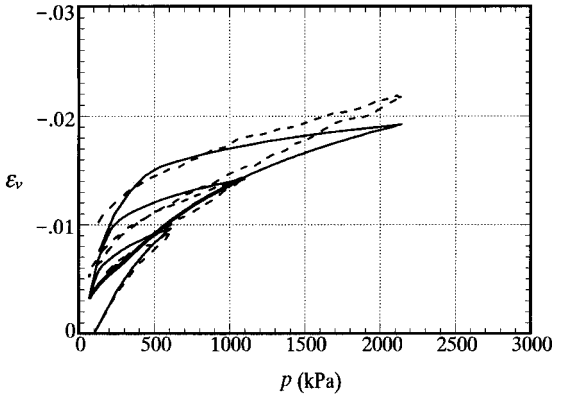

Figure 7. Cyclic isotropic loading by the true triaxial test apparatus

© 1998 John Wiley & Sons, Ltd.

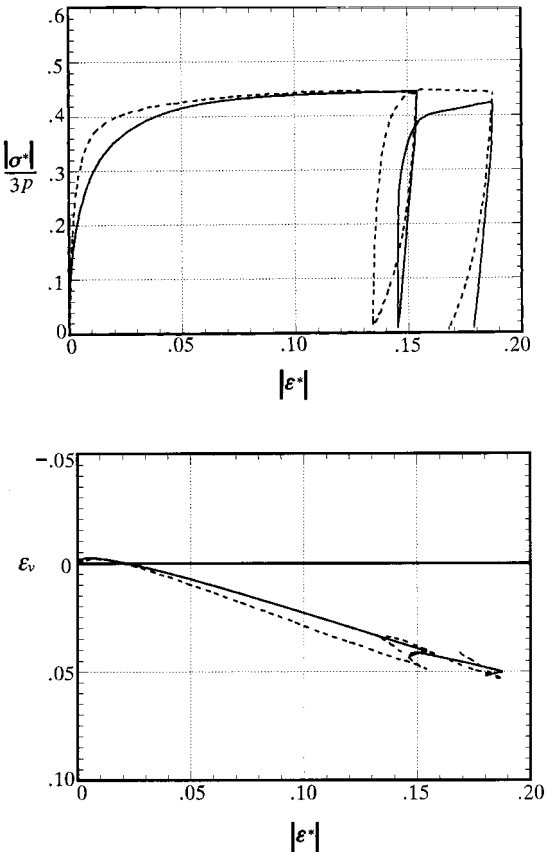

Figure 8. Axisymmetric compression with a constant lateral stress by the true triaxial test apparatus

shown in Figure 9. The response in unloading is predicted to be stiffer than the test data. The hysteresis loop with the reloading is shown for reference.

5.1.4. Proportional loading with b = 0·666 true triaxial test apparatus. The proportional loading with $b = 0.666(\theta_\sigma = -10^\circ 51')$ from $\boldsymbol{\sigma} = -500\mathbf{I}$ kPa is shown in Figure 10. That is, from the initial isotropic stress state of -500 kPa, the axial stress σ_z was increased by 330 to -170 kPa, while the lateral stress σ_x was decreased by $-165{\cdot}5$ to $-665{\cdot}5$ kPa proportionately keeping $d\sigma_x/d\sigma_z = -0{\cdot}5015$. The other stress σ_y was kept constant. All the principal strains and the volumetric strain are predicted to agree well with the test data.

5.1.5. Proportional loading with b = 0·286: hollow cylinder test apparatus. The proportional loading with $b = 0{\cdot}286$ from $\boldsymbol{\sigma} = -500\mathbf{I}$ kPa is shown in Figure 11. That is, from the initial isotropic stress state of -500 kPa, the shear stress $\tau_{\theta z}$ was increased to 450 kPa, while the axial stress σ_z was decreased by $-426{\cdot}1$ to $-926{\cdot}1$ kPa proportionately keeping $\tau_{\theta z}/\Delta\sigma_z = -1{\cdot}056$. The relations of the shear stress $\tau_{\theta z}$, the volumetric strain ε_v and the strain ε_z vs. the engineering

 © 1998 John Wiley & Sons, Ltd.

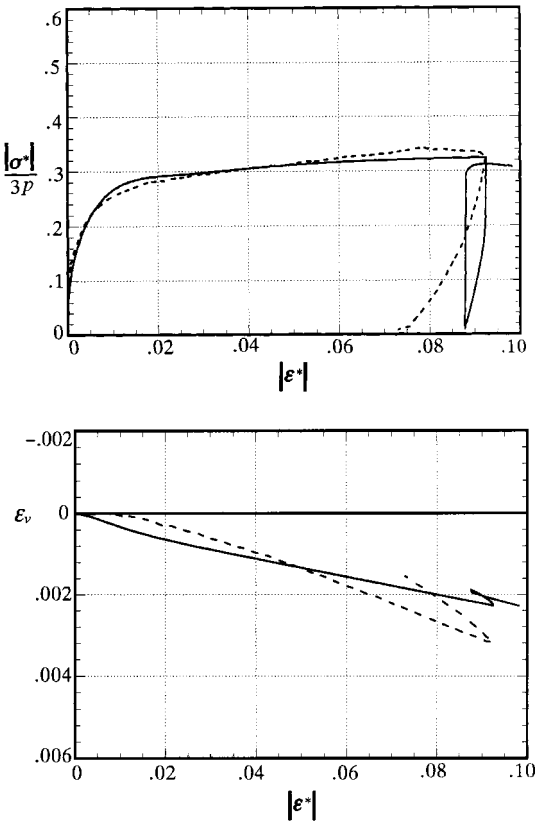

Figure 9. Axisymmetric extension with a constant lateral stress by the true triaxial test apparatus

shear strain $\gamma_{\theta z}$ ($\equiv 2\varepsilon_{\theta z}$) are depicted in the figure. The volumetric strain is predicted well but the shear stress $\tau_{\theta z}$ and the axial strain ε_z are predicted to be smaller than the test data.

5.1.6. Circular stress path in the deviatoric stress plane: true triaxial test apparatus. This test is split into two stages:

(i) The axial stress σ_z was decreased by -343 to -843 kPa from the isotropic stress state of -500 kPa, while σ_x and σ_y were both increased proportionately by 171 to -329 kPa, keeping the mean stress σ_m at -500 kPa. The magnitude of deviatoric stress $\|\boldsymbol{\sigma}^*\|$ finally became 420 kPa.

(ii) A circular stress path ($\theta_\sigma = 30 \rightarrow 750^\circ$) was depicted in a deviatoric stress plane by varying three principal stresses σ_x, σ_y, σ_z in sinusoidal forms, σ_m and $\|\boldsymbol{\sigma}^*\|$ being kept to be constant. The variations of the principal strains ε_x, ε_y, ε_z and the volumetric strain ε_v vs. the angle θ_σ for the circular stress path are shown in Figure 12. Variations of volumetric and principal strains are predicted well. The shape of the strain path in the deviatoric strain plane becomes a triangle. The sizes of the triangles in the test data and the calculation are almost identical, while their inclinations differ slightly from each other.

© 1998 John Wiley & Sons, Ltd.

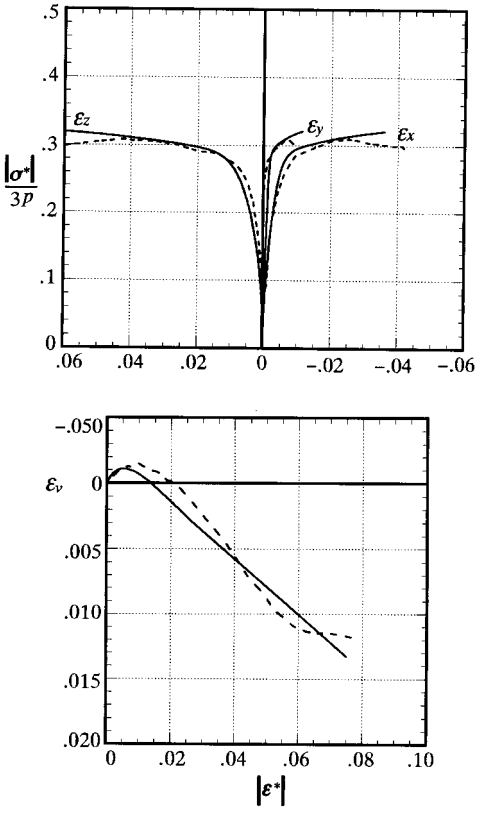

Figure 10. Proportional loading with $b = 0{\cdot}666$ by the true triaxial test apparatus

5.1.7. Cyclic torsional loading: hollow cylinder test apparatus. The cyclic torsional loading (5 cycles) between the shear stress limits $\tau_{\theta z} = \pm 135\,\mathrm{kPa}$ under $\sigma_r = \sigma_\theta = -500\,\mathrm{kPa}$ and $\sigma_z = -1{,}020\,\mathrm{kPa}$ loaded from the isotropic stress state $\boldsymbol{\sigma} = -500\mathbf{I}\,\mathrm{kPa}$ is shown in Figure 13. The shake down of the hysteresis loop is brought about more gradually in the calculated result than in the test data.

5.2. Undrained tests

The applicability of the present model to the prediction of the undrained behaviour of sands is examined comparing with the test data in the axisymmetric stress state by the triaxial test apparatus.

5.2.1. Monotonic loading. The test data[30] and the calculated results of the stress paths in the (p, q) plane and the relations of q vs. the axial strain ε_a for the monotonic loading in the axisymmetric compression under the undrained condition are shown in Figure 14. The material is Banding sand with the initial relative densities $D_r = 0{\cdot}27, 0{\cdot}44, 0{\cdot}47, 0{\cdot}64$ under the initial pressure

 © 1998 John Wiley & Sons, Ltd.

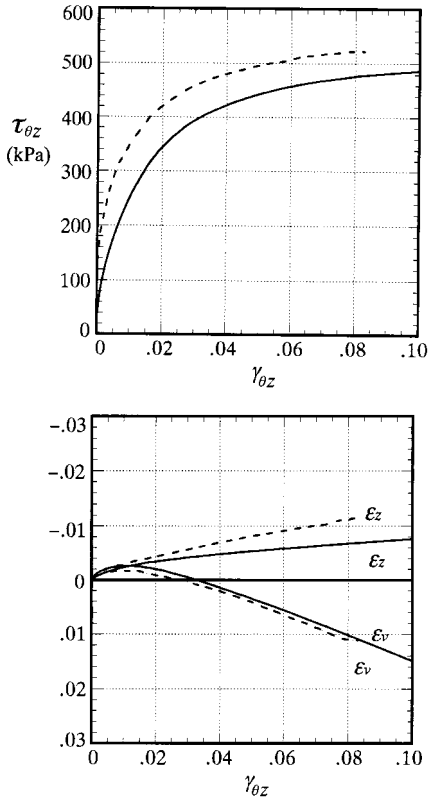

Figure 11. Proportional loading with $b = 0{\cdot}286$ by the hollow cylinder test apparatus

$p_0 = 400\,\mathrm{kPa}$. Material constants and initial values for the calculation are selected as follows:

material constants:

yield surface (ellipsoid) shape $\phi = 26, 30, 31, 32^\circ$

$$\text{hardening/softening} \begin{cases} \text{isotropic} \begin{cases} \text{volumetric} & \rho = 0{\cdot}025, 0{\cdot}018, 0{\cdot}014, 0{\cdot}010 \\ & p_i = 0, 10, 30, 80\,\mathrm{kPa} \\ \text{deviatoric} & \mu = 1{\cdot}00, 0{\cdot}65, 0{\cdot}30, 0{\cdot}10 \\ & \phi_d = 40, 33, 30, 20^\circ \end{cases} \\ \text{rotational} \quad b_r = 10,\ \phi_b = 20^\circ \end{cases}$$

evolution of R: $u_1 = 0{\cdot}1, 0{\cdot}3, 0{\cdot}5, 1{\cdot}0, m_1 = 0{\cdot}1, 0{\cdot}4, 0{\cdot}5, 0{\cdot}7$
movement of similarity-centre $c = 20, 18, 14, 8$
elastic constants: $\gamma = 0{\cdot}0067, 0{\cdot}0065, 0{\cdot}0060, 0{\cdot}0058,$
$G = 18,000, 23,000, 25,000, 35,000\,\mathrm{kPa}$

© 1998 John Wiley & Sons, Ltd.

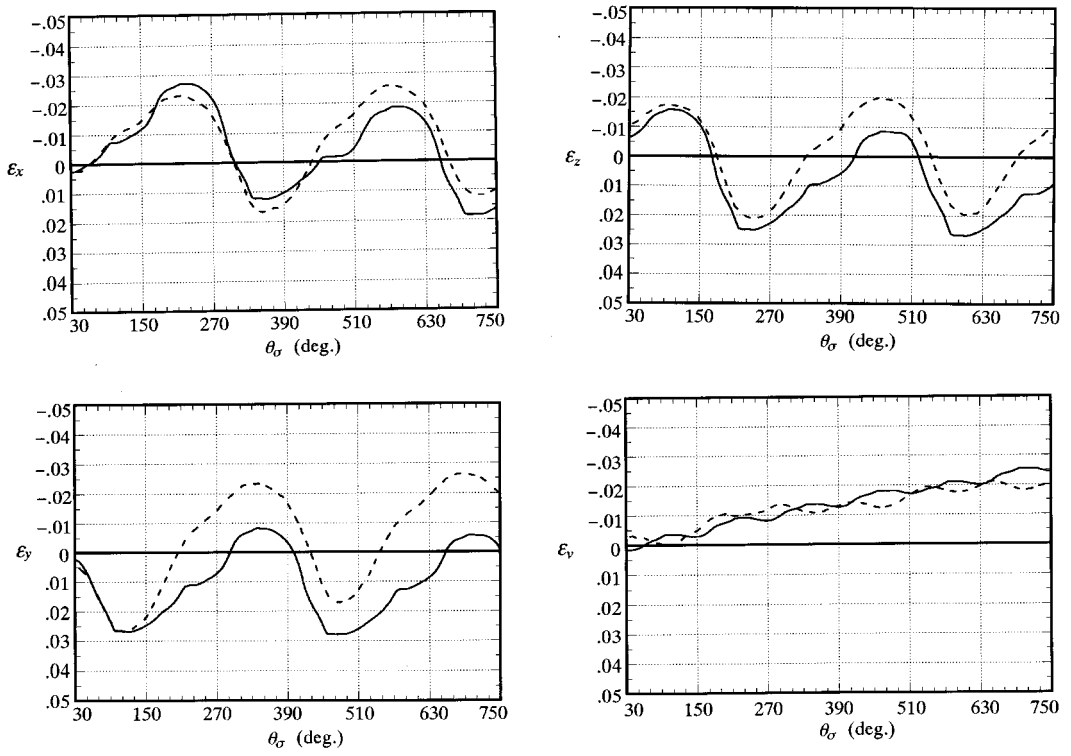

Figure 12. Variations of three principal strains ε_x, ε_y, ε_z and volumetric strain ε_v vs. angle θ_σ for the loading of circular stress path in the deviatoric stress plane by the true triaxial test apparatus

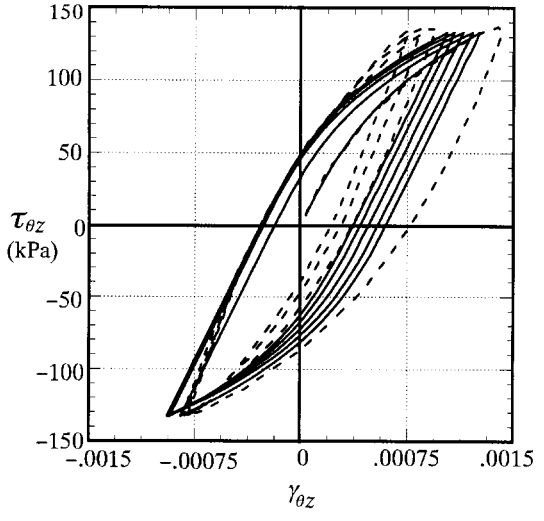

Figure 13. Cyclic torsional loading by the hollow cylinder test apparatus

 © 1998 John Wiley & Sons, Ltd.

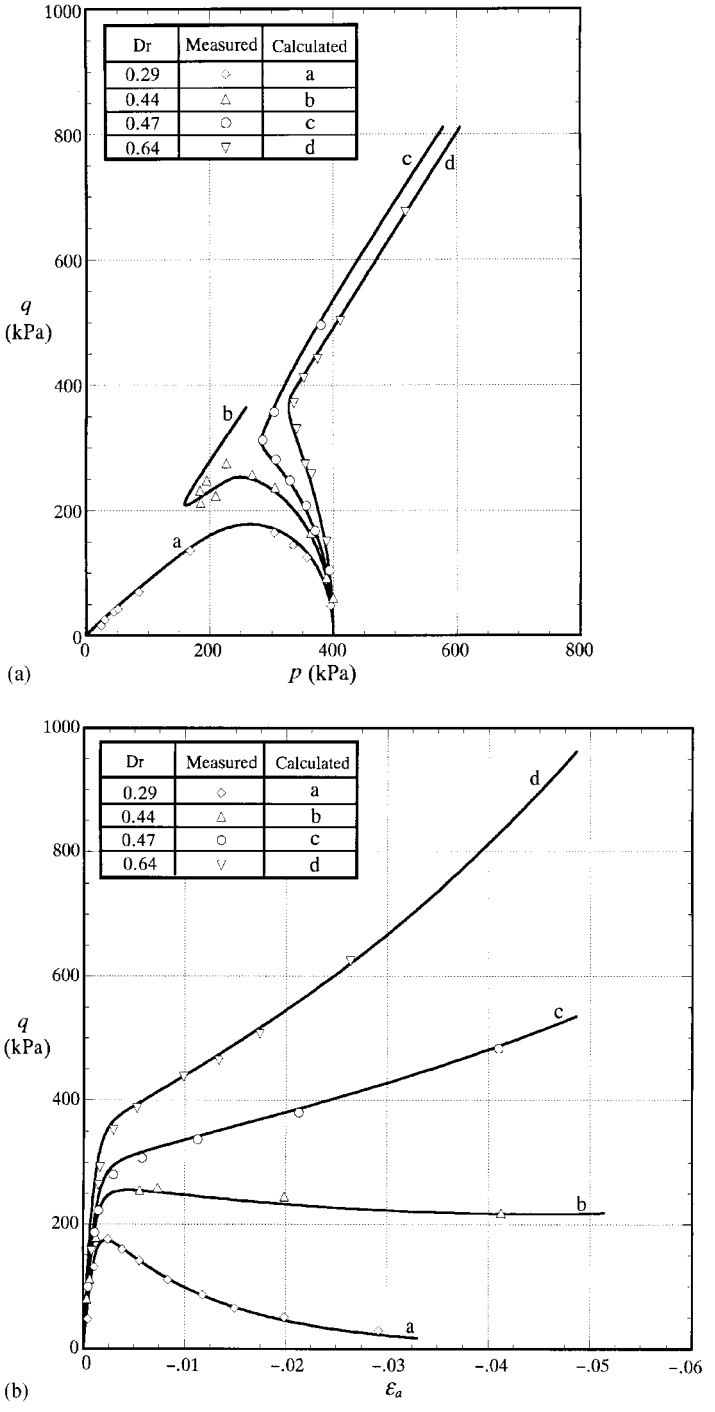

Figure 14. Undrained behaviour of Banding sand (data from Castro [30]). Calculated results are shown by solid lines

© 1998 John Wiley & Sons, Ltd.

initial values:

$$F_0 = 410, 480, 520, 580\,\mathrm{kPa},\ \boldsymbol{\beta}_0 = \mathbf{O},\ \mathbf{s}_0 = -200, -110, -100, -80\mathbf{I}\,\mathrm{kPa},$$
$$\boldsymbol{\sigma}_0 = -400\mathbf{I}\,\mathrm{kPa}$$

where the four numbers written for constants or an initial value correspond to the case of $D_r = 0{\cdot}27, 0{\cdot}44, 0{\cdot}47, 0{\cdot}64$, respectively, in this order.

Fairly good agreements between the test data and the calculated results are realized.

5.2.2. Cyclic mobility. The test data[31,33] and the calculated results of the stress path and the stress–strain relation for the cyclic mobility with the constant stress amplitude $q = \pm 0{\cdot}71\,\mathrm{kgf/cm^2}$ in the axisymmetric compression under the undrained condition are shown in Figure 15. The material is Niigata sand with the initial void ratio $e_0 = 0.737$ under the initial pressure $p_0 = 2.1\,\mathrm{kgf/cm^2}$. The following material constants and initial values are used in the calculation.

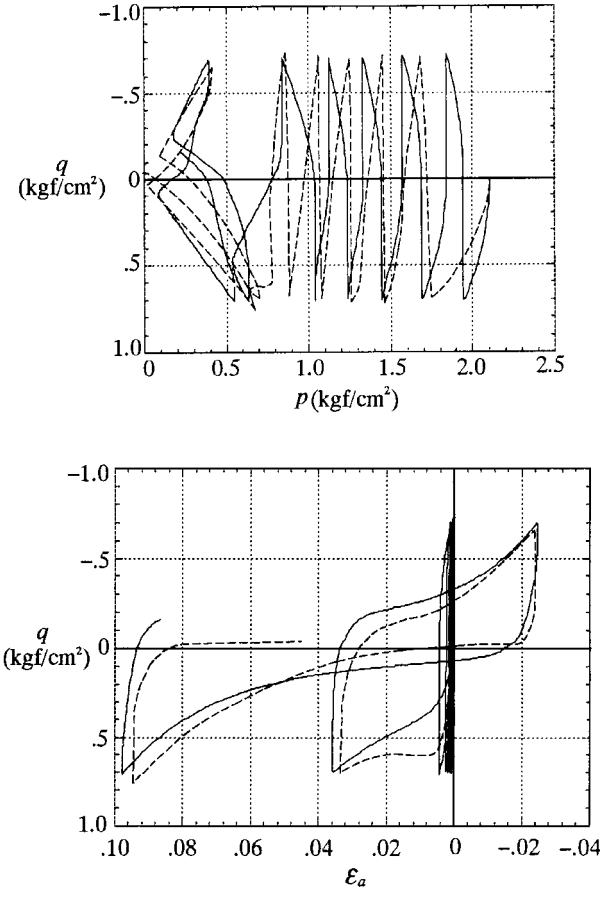

Figure 15. Cyclic mobility of loose Niigata sand (after Tatsuoka[31] or Ishihara *et al.*[33]). Test data and calculated results are depicted by dashed and solid lines, respectively

 © 1998 John Wiley & Sons, Ltd.

material constants:

$$\text{yield surface (ellipsoid) shape } \phi = 28^\circ$$

$$\text{hardening/softening} \begin{cases} \text{isotropic} \begin{cases} \text{volumetric } \rho = 0{\cdot}01,\ p_i = 0{\cdot}05\,\text{kgf/cm}^2 \\ \text{deviatoric } \mu = 1{\cdot}0,\ \phi_d = 35^\circ \end{cases} \\ \text{rotational } b_r = 120,\ \phi_b = 35^\circ \end{cases}$$

$$\text{evolution of } R\text{: } u_1 = 8{\cdot}0,\ m_1 = 1{\cdot}3$$
$$\text{movement of similarity-centre } c = 34$$
$$\text{elastic constants: } \gamma = 0{\cdot}0065,\ G = 1800\,\text{kgf/cm}^2$$

initial values:

$$F_0 = 5{\cdot}5\,\text{kgf/cm}^2,\ \boldsymbol{\beta}_0 = \mathbf{O},\ \mathbf{s}_0 = -0{\cdot}2\mathbf{I}\,\text{kgf/cm}^2,$$
$$\boldsymbol{\sigma}_0 = -2{\cdot}1\mathbf{I}\,\text{kgf/cm}^2$$

Good agreement between the test data and the calculated results is observed in the figures.

6. MECHANICAL FEATURES OF THE PRESENT MODEL

The elastoplastic constitutive equation of soils with the subloading surface and the rotational hardening was proposed in this article. Main features of this model are as follows:

(1) As was described in the previous article,[18] this model fulfills the *condition of continuity*

$$\mathring{\boldsymbol{\sigma}}(\boldsymbol{\sigma} + \delta\boldsymbol{\sigma}, \mathbf{H}_i, \mathbf{D}) - \mathring{\boldsymbol{\sigma}}(\boldsymbol{\sigma} + \mathbf{H}_i, \mathbf{D}) \to \mathbf{O} \quad \text{for } \delta\boldsymbol{\sigma} \to \mathbf{O} \tag{78}$$

and also the *smoothness condition*

$$\lim_{\delta\boldsymbol{\sigma}\to\mathbf{O}} \frac{\partial\mathring{\boldsymbol{\sigma}}(\boldsymbol{\sigma} + \delta\boldsymbol{\sigma}, \mathbf{S}_i, \mathbf{D})}{\partial\mathbf{D}} = \frac{\partial\mathring{\boldsymbol{\sigma}}(\boldsymbol{\sigma}, \mathbf{S}_i, \mathbf{D})}{\partial\mathbf{D}} \tag{79}$$

for a monotonic loading process so that the smooth elastic–plastic transition is described, where the response of stress rate to the input of stretching for the current stress and internal state variables is designated as $\mathring{\boldsymbol{\sigma}}(\boldsymbol{\sigma}, \mathbf{S}_i, \mathbf{D})$, $\mathbf{S}_i$ $(i = 1, 2, \ldots, n)$ denoting collectively scalar- or tensor-valued plastic internal state variables.

Conventional plasticity in which the interior of the yield surface is assumed to be an elastic domain violates the smoothness condition (79), and thus it is required to incorporate the algorithms for judging the fulfillment of the yield condition and for selecting a stress increment for which a stress does not go out from the yield surface, e.g. the *Euler method*,[34] the *mean normal method*[35] and the *radial return method*,[36] in computer programs. On the other hand, the subloading surface model fulfills the smoothness condition, and thus it is not required to judge the fulfillment of the yield condition, having the controlling function to pull back automatically the stress to the normal-yield surface when it goes out from the surface.[18] While the smoothness condition does not have a substantial influence on a prediction of monotonic loading behaviour,

© 1998 John Wiley & Sons, Ltd.

it is important for a prediction of cyclic loading behaviour requiring a delicate prediction of small strain accumulation, repeating a loading and an unloading.

(2) The similarity-centre of the normal-yield and the subloading surfaces moves as a plastic deformation occurs. The *Masing effect* is controllable by the selection of the material constant c in equation (44) so that the hysteresis loop is depicted realistically,[18] leading to the pertinent description of cyclic loading behaviour of materials. On the other hand, the initial subloading surface model or the bounding surface model with a radial mapping in which the similarity-centre is fixed is incapable of describing cyclic loading behaviour realistically, predicting an excessive strain accumulation with open hysteresis loops for stress amplitudes of entirely positive or entirely negative one side since the similarity-centre is fixed in the origin of stress space or in the particular reference point within a yield surface.[18]

(3) Almost all elastoplastic constitutive equations of soils adopt the non-associated flow rule with a plastic potential surface which is different from the yield surface, although the non-associated flow rule has the mechanical peculiarity violating the *work rate-stiffness relaxation*,[17,37,38] i.e. exhibiting a larger second-order work rate for a certain stretching and a larger stiffness modulus in the elastoplastic process than in the elastic process. Also, it induces the loss of the symmetry of the elastoplastic modulus tensor (fourth-order), which leads to an inconvenience in the analysis of boundary value problems. They assume a conical yield surface such as the extended Mises yield surface or a similar one for states denser than critical state (overconsolidated state for clays). An unrealistically large plastic volumetric expansion is predicted when the associated flow rule is applied to such a yield surface. On the other hand, the plastic volumetric expansion predicted by the initial subloading surface model in which a similarity-centre is fixed in the origin of stress space is far smaller than that predicted by the extended Mises yield surface with the associated flow rule as shown in Figure 16(a). Further, the outward normal of the subloading surface can have a negative component of the hydrostatic axis causing plastic volumetric contraction by the associated flow rule even for states denser than critical state in the (extended) subloading surface model in which the similarity-centre moves with a plastic deformation as shown in Figure 16(b). Besides, a stress turns back at the moment fulfilling $D_p = 0$ in equation (55) before it reaches the normal-yield surface, approaching finally the critical state in axisymmetric compression with a constant lateral stress under a drained condition for example.[7,8] Thus, the subloading surface model would not predict the volumetric expansion to be excessively large.

(4) A single equation of an ellipsoid is incorporated for normal-yield and subloading surfaces without a plastic potential surface different from the subloading surface. The evolutional rule for the movement of the similarity-centre is pertinently given by the simple equation derived so as to fulfill the enclosing condition of the similarity-centre. The plastic modulus is pertinently formulated from the extended consistency condition for the subloading surface, incorporating the evolutional rule of the variable R.

(5) Rotational hardening is incorporated and its evolutional rule is formulated in order to describe the inherent and the induced anisotropy.

(6) The linear relation between the void ratio and the pressure for the isotropic consolidation has been widely used in constitutive equations of soils since the Cam-clay model. However, it is not applicable to the state in which a mean stress is small since it has the unrealistic characteristics that the void ratio becomes infinite for the state in which a mean stress is zero. Also, it is inapplicable to large deformation problems.[29] On the other hand, the linear relation between the volume and the pressure used in the present model does not have these defects.

 © 1998 John Wiley & Sons, Ltd.

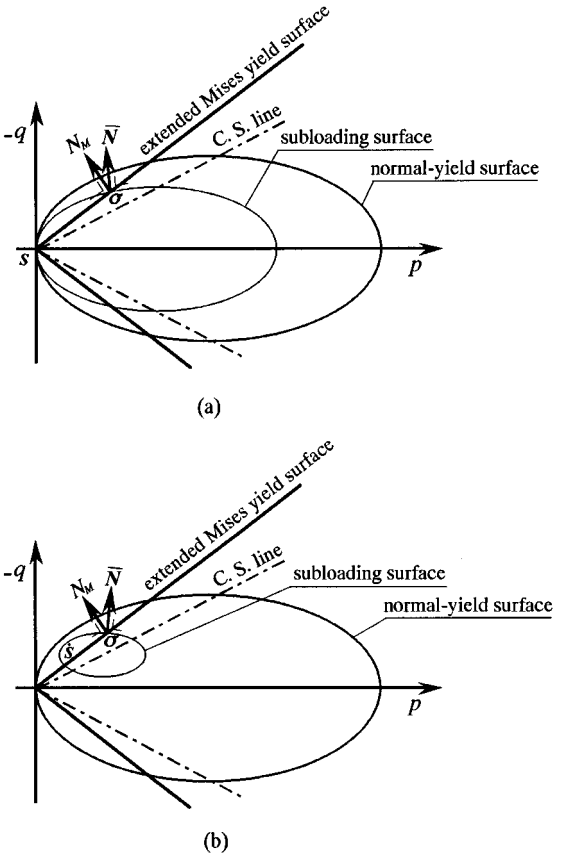

Figure 16. The outward-normal $\mathbf{N}_M$ and $\bar{\mathbf{N}}$ of the extended von Mises yield surface and (a) the initial or (b) (extended) subloading surface

7. ON THE OTHER MODELS FOR SOILS

Various elastoplastic constitutive models which are aimed at predicting a cyclic loading behaviour of soils have been proposed in the past. The deformation behaviour of sands is more complicated than that of clays. In this section popular models developed for cyclic loading behaviour of sands are classified according to their mechanical structures and their mechanical characteristics are examined, while general features of cyclic plasticity models have been described in some articles.[17,18]

7.1. Bounding surface model with a radial mapping (initial subloading surface model)

The bounding surface model with a radial mapping[15] falls within the framework of the initial subloading surface model[7,8] but the plastic modulus is given *a priori* by the interpolation method, while the plastic modulus is formulated pertinently by the extended consistency condition in the initial subloading surface model (equation (52) in the present model). It has been applied to both

© 1998 John Wiley & Sons, Ltd.

clays and sands by Bardet[39,40] and Crouch and Wolf.[41,42] The proposed constitutive equations obey the nonassociated flow rule with bounding and plastic potential surfaces in complicated shapes, which induce mechanical peculiarity.[17,37,38] The similarity-centre of the normal-yield (bounding) surface and the subloading (loading) surfaces is fixed in the constitutive equation of Bardet. Therefore, an excessive strain accumulation with open hysteresis loops is predicted for cyclic loading with stress amplitudes in entirely positive or entirely negative one side. Thus, his model would be unable to predict pertinently the deformation behaviour shown in Figures 7–9. The similarity-centre (projection-centre) moves in very limited manner and range in the constitutive equation of Crouch and Wolf, while different rules for the movement are assumed in the radial and the deviatoric mapping regions. These patchwork structures lead to the violations of the continuity condition (78) and the smoothness condition (79). It could describe a cyclic loading behaviour only for stress amplitudes including the special range where the similarity-centre is movable, predicting a closed hysteresis loop. The assumed normal-yield surface has an isotropic shape, the central axis being fixed to coincide with the hydrostatic axis. Therefore, the anisotropy is not taken into account.

7.2. Bounding surface model with a radial mapping and a rotational hardening

Rotational hardening has been incorporated into the bounding surface model with radial mapping for sands and clays by Banerjee and Yousif[43], Liang and Shaw[44] and Liang and Ma[45]. This modification allows the bounding surface model with radial mapping to describe inherent and induced anisotropy. However, the rotation of surface is accounted only for the anisotropic consolidation process in the constitutive equation of Banerjee and Yousif. On the other hand, the fact (4) in Section 2 for anisotropic consolidation is not taken into account in the evolutional rule of the rotational hardening in the constitutive equations of Liang and Shaw and Liang and Ma. Therefore, it leads to the unrealistic behaviour that, in the anisotropic consolidation process of initially isotropic materials, the centre of the normal-yield surface continues to rotate crossing the anisotropic consolidation line in the stress space. The similarity-centre is fixed at a special point on the central axis of the normal-yield surface in these equations so that an excessive strain accumulation with open hysteresis loops is predicted for the cyclic loading in which the magnitude of stress remains in entirely positive or entirely negative one side. Further, the critical state surface assumed in the constitutive equation becomes concave in the case that the angle of internal friction for that state is larger than $22^\circ 01'$ (cf. Reference 46).

7.3. Generalized plasticity

Zienkiewicz and Mroz[47] proposed the novel concept for cyclic loading behaviour, which assumes that a plastic deformation is induced even by a stress rate directed towards as interior of yield or loading surface, adopting a larger plastic modulus than that in the case of stress rate directed towards an exterior of that surface. A similar concept has been proposed before then by Aboim and Roth[48] and Pande and Pietruszczak.[49] Attempts have been made to apply this concept to the prediction of soil deformation behaviour by some workers.[47–53] Zienkiewicz and Mroz[47] called it *generalized plasticity*. However, it exhibits various unrealistic characteristics:

(i) A larger plastic stretching is induced by a stress rate directed towards a more interior of a yield or loading surface as illustrated in Figure 17. Namely, a plastic deformation is not

 © 1998 John Wiley & Sons, Ltd.

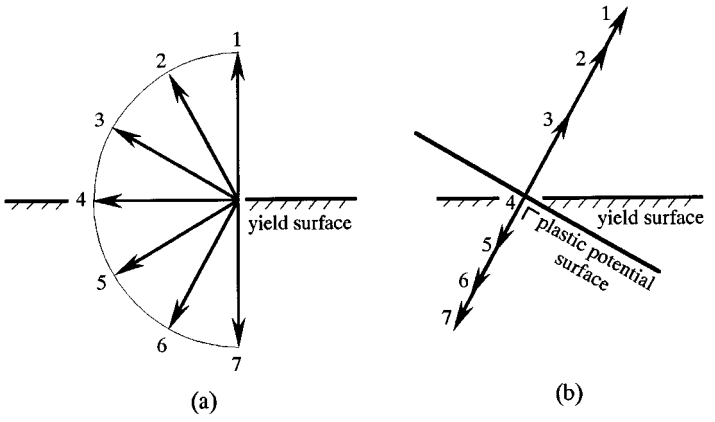

Figure 17. The peculiarity of the generalized plasticity: (a) stress rates $\mathring{\boldsymbol{\sigma}}$ as inputs and (b) plastic stretching $\mathbf{D}^{\mathrm{p}}$ as responses. A larger plastic stretching is induced by a stress rate directed towards a more interior of a yield or loading surface

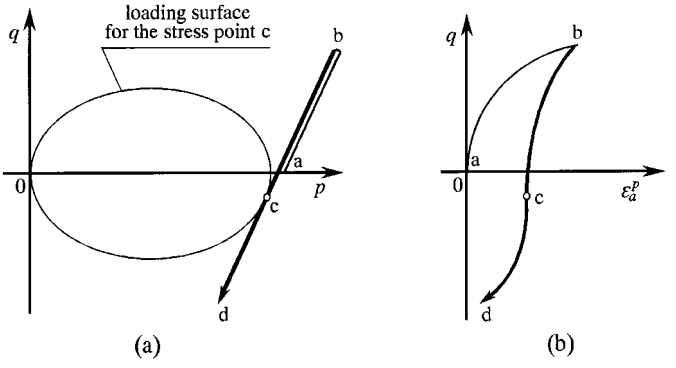

Figure 18. The another peculiarity of the generalized plasticity: An inflection (point c in (b)) appears in the stress–strain curve of the unloading process: (a) the stress path in the (p, q) plane and (b) the stress–plastic strain curve in the $(\varepsilon_a^p, \mathrm{q})$ plane (ε_a^p: plastic axial strain)

induced by the stress rate tangential to that surface, causing the neutral loading, but the largest plastic deformation is done by the stress rate directed towards the inward normal of that surface.

(ii) An inflection appears in the stress–strain curve of the unloading process along a straight stress path, since a plastic deformation is predicted just after the incipience of the unloading process but only an elastic deformation is predicted when the direction of the stress rate becomes tangential to a loading surface as illustrated in Figure 18 for the triaxial compression with a constant lateral stress for instance.

(iii) An excessive strain accumulation with open hysteresis loops is predicted for cyclic loading with stress amplitudes in entirely positive or entirely negative one side, since the similarity-centre of the normal-yield and the subloading surfaces is fixed in the origin of stress space.

© 1998 John Wiley & Sons, Ltd.

Therefore, this model is unable to predict realistically the deformation behaviour shown in Figures 7–9.

(iv) The non-associated flow rule is adopted so that the mechanical peculiarity[17,37,38] and the inconvenience in the analysis of boundary value problems are caused.

(v) The assumed normal-yield surface has an isotropic shape, the central axis being fixed to coincide with the hydrostatic axis. Therefore, anisotropy is not taken into account. Besides, the critical state surface assumed in the constitutive equation becomes concave in the case that the angle of internal friction for that state is larger that 22°01′.

7.4. Rotation of conical yield surface

Soil models involving the rotation of a conical yield surface within a conical failure surface have been studied by some workers.[54–57] These models may fall within the framework of the two surface model type. Therefore, excessive strain accumulation with open hysteresis loops is predicted for a cyclic loading with stress amplitudes in entirely positive or entirely negative one side.[18] Also, it is inapplicable to the prediction of a cyclic proportional loading behaviour, i.e. a cyclic isotropic or anisotropic consolidation, predicting an elastic behaviour for stress amplitudes less than the maximum one in a deformation history.

7.5. Multi-surface model

The multi-surface, model[1,2] has been applied to soils by some workers.[58–60] However, this model does not have a pertinent structure for describing a cyclic loading behaviour, predicting very unrealistic behaviour as was indicated by Hashiguchi.[18] For instance, the mechanical ratchetting, i.e. the strain accumulation is not predicted but the inverse mechanical ratchetting, i.e. the strain decrease is predicted for cyclic loading with a constant stress amplitude in a hardening process.

7.6. Hierarchical single-surface model and disturbed-state concept

The hierarchical single-surface model and the disturbed-state concept[61–63] developed by Desai and his colleagues provide the novel constitutive equations in which a small plastic potential surface is assumed in order to describe the sophisticated non-associated flow rule and the induced anisotropy, incorporating pertinent yield surface and hardening rule. They could predict realistically the deformation of clays and sands, including their cyclic loading behaviour.

The above-mentioned models for a cyclic loading behaviour fall within the framework of the plasticity premising the existence of a yield surface and the decomposition of stretching into the elastic and the plastic parts for describing a plastic deformation history through plastic internal state variables. On the other hand, some models different from the plasticity, e.g. the endochronic theory and the non-linear rate (hypoplastic) models have been proposed (cf. reference. 64). They are not reviewed in this article, however.

8. CONCLUDING REMARKS

An elastoplastic constitutive equation was formulated in this article, which has a modular structure of several pertinent concepts, i.e. an associated flow rule, a subloading surface,

 © 1998 John Wiley & Sons, Ltd.

rotational hardening, etc., and rather simple forms despite of the comprehensive capability. It was applied to the prediction of the deformation behaviour of sands for various kinds of loading from isotropic to deviatoric stress state including cyclic loading, and thus its applicability was verified for a wide range of loading processes. This equation is also valid for clays in the present form by putting the material constant $\mu = 0$ in the isotropic hardening rule (73), while it was verified even by the old form without a rotational hardening.[21] However, it is desirable to improve the constitutive equation by due consideration of the physical meanings of material functions and the determination of material constants.

REFERENCES

1. Z. Mroz, 'On the description of anisotropic hardening', *J. Mech. Phys. Solids*, **15,** 163–175 (1967).
2. W. D. Iwan, 'On a class of models for the yielding behavior of continuous and composite systems'. *J. Appl. Mech. ASME*, **34,** 612–617 (1967).
3. Y. F. Dafalias and E. P. Popov, 'A model of nonlinearly hardening materials for complex loading', *Acta Mech.*, **23,** 173–192 (1975)
4. R. D. Krieg, 'A practical two surface plasticity theory', *J. Appl. Mech. ASME*, **42,** 641–646 (1975)
5. Y. F. Dafalias and E. P. Popov, 'Cyclic loading for materials with a vanishing elastic domain', *Nucl. Engng. Des.*, **41,** 293–302 (1977).
6. Z. Mroz, V. A. Norris and O. C. Zienkiewicz, 'An anisotropic, critical state model for soils subjected to cyclic loading', *Geotechnique*, **31,** 451–469 (1981).
7. K. Hashiguchi, and M. Ueno 'Elastoplastic constitutive laws of granular materials'. in S. Murayama and A. N. Schofield (eds), *Constitutive Equations of Soils*, *Proc. 9th Int. Conf. Soil Mech. Found. Eng.*, *Spec. Session* 9, Tokyo, JSSMFE, Tokyo, 1977, pp.73–82.
8. K. Hashiguchi, 'Constitutive equations of elastoplastic materials with elastic–plastic transition', *J. Appl. Mech. ASME*, **47,** 266–272 (1980)
9. K. Hashiguchi, 'Subloading surface model in unconventional plasticity', *Int. J. Solids Struct.*, **25,** 917–945 (1989)
10. P. J. Armstrong and O. C. Frederick, 'A mathematical representation of the multiaxial Bauschinger effect', *C.E.G.B. Report RD/B/N*731, Central Electricity Generating Board, 1966.
11. J. L. Chaboche, 'Viscoplastic constitutive equations for the description of cyclic and anisotropic behavior of metals'. *Bull. Acad. Polon. Sci. Ser. Sci. Tech.*, **25,** 1977.
12. D. Marquis, 'Modelisation et identification de l'ecrouissage anisotrope des metaux', *These Paris VI*, 1979.
13. J. L. Chaboche and G. Rousselier, 'On the plastic and viscoplastic constitutive equations', *J. Pressure Vessel Tech. ASME*, **105,** 153–164 (1983).
14. T. Ohno and J. -D. Wang, 'Transformation of a nonlinear kinematic hardening rule to a multisurface form under isothermal and nonisothermal conditions'. *Int. J. Plasticity*, **7,** 879–892 (1993).
15. Y. F. Dafalias and L. R. Herrmann, 'A bounding surface soil plasticity model', in G. N. Pande and O. C. Zienkiewicz (eds), *Proc. Int. Symp. Soils under Cyclic Trans. Load.*, Swansea, A. A. Balkema, Rotterdam, 1980, pp. 335–345.
16. K. Hashiguchi, 'Macrometric approaches —static— intrinsically time-independent', in S. Murayama (ed.), *Constitutive Laws of Soils*, *Proc. 11th Int. Conf. Soil, Mech. Found. Engng.*, *Spec. Session* 9, Tokyo, JSSMFE, Tokyo, 1985, pp. 25–65.
17. K. Hashiguchi, 'Fundamental requirements and formulation of elastroplastic constitutive equations with tangential plasticity', *Int. J. Plasticity*, **9,** 525–549 (1993).
18. K. Hashiguchi, 'Mechanical requirements and structures of cyclic plasticity models', *Int. J. Plasticity*, **9,** 721–748 (1993).
19. K. Hashiguchi and T. Yoshimaru, 'A generalized formulation of the concept of nonhardening region', *Int. J. Plasticity*, **11,** 347–365 (1995).
20. K. Hashiguchi, M. Ueno and T. Imamura, 'Prediction of deformation behavior of sands by the subloading surface model', in A. S. Saada and G. Bianchini (eds), *Proc. Int. Workshop on Constitutive Equations for Granular Noncohesive Soils*, Cleveland, A. A. Balkema, Rotterdam, 1989, pp. 293–306.
21. M. Topolnicki, 'An elasto-plastic subloading surface model for clay with isotropic and kinematic mixed hardening parameters', *Soils Found.*, **30,** 103–113 (1990).
22. H. Sekiguchi and H. Ohta, 'Induced anisotropy and time dependency in clays', in S. Murayama and A. N. Schofield (eds), *Constitutive Equations of Soils*, *Proc. 9th Int. Conf. Soil Mech. Found. Eng.*, *Spec. Session 9*, Tokyo, JSSMFE, Tokyo, 1977, pp. 229–238.

© 1998 John Wiley & Sons, Ltd.

23. K. Hashiguchi, 'An expression of anisotropy in a plastic constitutive equation of soils', S. Murayama and A. N. Schofield (eds), *Constitutive Equations of Soils*, *Proc. 9th Int. Conf. Soil Mech. Found. Eng.*, *Spec. Session 9*, Tokyo, JSSMFE, Tokyo, 1977, pp. 302–305.
24. K. Hashiguchi, 'Constitutive equations of granular media with an anisotropic hardening', in W. Wittke (ed.), *Proc. 3rd Int. Conf. Numer. Meth. Geomech.*, Aachen, A. A. Balkema, Rotterdam, 1979, pp. 435–439
25. R. Hill, 'A general theory of uniqueness and stability in elastic-plastic solids', *J. Mech. Phys. Solids*, **6,** 236–249 (1958).
26. R. Hill, 'On the classical constitutive relations for elastic/plastic solids', *Recent Progress in Appl. Mech.* (*The Folke Odqvist Volume*), Wiley, New York, 1967, pp.241–249.
27. K. Hashiguchi, 'On the loading criterion', *Int. J. Plasticity*, **10,** 871–878 (1994).
28. K. Hashiguchi, 'Isotropic hardening theory of granular media', *Proc. JSCE*, **227,** 45–60 (1974).
29. K. Hashiguchi, 'On the linear relations of V-ln$p$ and ln$v$-ln$p$ for isotropic consolidation of soils', *Int. J. Numer. Analyt. Meth. Geomech.*, **19,** 367–376 (1995).
30. G. Castro, 'Liquefaction of sands', *Ph.D. Thesis*, Harvard Soil Mech. Series, No. 81, 1969.
31. F. Tatsuoka, 'Study on deformation characteristics of sand by triaxial tests', *Doctor Thesis*, Tokyo University, 1972.
32. A. S. Saada and G. Bianchini (eds), *Proc. Int. Workshop on Constitutive Equations for Granular Non-cohesive Soils*, Cleveland, Balkema, Rotterdam, 1989.
33. K. Ishihara, F. Tatsuoka and S. Yasuda, 'Undrained deformation and liquefaction of sand under cyclic stresses', *Soils Found.*, **15,** 29–44 (1975).
34. Y. Yamada, N. Yoshimura and T. Sakurai, 'Plastic stress-strain matrix and its application for the solution of elastic-plastic problems by finite element method', *Int. J. Mech. Sci.*, **10,** 343–354 (1968).
35. R. D. Krieg and D. B. Krieg, 'Accuracies of numerical solution methods for the elastic-perfectly plastic models', *J. Pressure Vessel Tech. ASME*, **99,** 510–515 (1977).
36. I. Pillinger, P. Hartley, C. E. N. Sturgess and G. W. Rowe, 'Use of a mean-normal large-strain elastic-plastic finite-element solutions', *Int. J. Mech. Sci.*, **28,** 23–29 (1986).
37. K. Hashiguchi, 'Inexpedience of the nonassociated flow rule', *Int. J. Numer. Analyt. Meth. Geomech.*, **15,** 752–756 (1991).
38. K. Runesson and Z. Mroz, 'A note on nonassociated flow rules', *Int. J. Plasticity*, **5,** 639–658 (1989).
39. J. P. Bardet, 'Bounding surface plasticity model for sands', *J. Eng. Mech. ASCE*, **112,** 1198–1217 (1986).
40. J. P. Bardet, 'Hypoplastic model for sands', *J. Eng. Mech. ASCE*, **116,** 1973–1994 (1990).
41. R. S. Crouch and J. P. Wolf, 'Unified 3D critical state bounding-surface plasticity model for soils incorporating continuous plastic loading under cyclic paths. Part I: constitutive relations', *Int. J. Numer. Analyt. Meth. Geomech.*, **18,** 735–758 (1994).
42. R. S. Crouch and J. P. Wolf, 'Unified 3D critical state bounding-surface plasticity model for soils incorporating continuous plastic loading under cyclic paths. Part II: calibration and simulations', *Int. J. Numer. Analyt. Meth. Geomech.*, **18,** 759–784 (1994).
43. P. K. Banerjee and N. B. Yousif, 'A plasticity for the mechanical behaviour of anisotropically consolidated clay', *Int. J. Numer. Analyt. Meth. Geomech.*, **10,** 521–541 (1986).
44. R. Y. Liang and H. -L. Shaw, 'Anisotropic hardening plasticity model for sands', *J. Geotech. Eng. ASCE*, **117,** 913–933 (1991).
45. R. Y. Liang and F. Ma, 'Anisotropic hardening plasticity model for undrained cyclic behavior of clays. I: theory', *J. Eng. Mech. ASCE*, **118,** 229–245 (1992).
46. K. Hashiguchi, 'Theories of yielding for frictional materials', *Proc. JSCE*, **199,** 57–66 (1972).
47. O. C. Zienkiewicz and Z. Mroz, 'Generalized plasticity formulation and application to geomechanics', in C. S. Desai and R. H. Gallagher (eds), *Mech. Engng. Materials*, Wiley, Newyork, 1984, pp. 655–679.
48. C. A. Aboim and W. H. Roth, "Bounding-surface-plasticity theory applied to cyclic loading of sand", in R. Dungar, G. N. Pande and J. A. Studer (eds), *Int. Symp. Numer. Models in Geomech.*, A. A. Balkema, Rotterdam, 1982, pp. 65–80.
49. G. N. Pande and St. Pietruszczak, "Reflecting surface" model for soils', R. Dungar, G. N. Pande and J. A. Studer (eds), *Int. Symp. Numer. Models in Geomech.*, A. A. Balkema, Rotterdam, 1982, pp. 50–64.
50. O. C. Zienkiewicz, K. H. Leung and M. Pastor, 'Simple model for transient soil loading in earthquake analysis. I. Basic model and its application', *Int. J. Numer. Analyt. Meth. Geomech.*, **9,** 453–476 (1985).
51. M. Pastor, O. C. Zienkiewicz and K. H. Leung, 'Simple model for transient soil loading in earthquake analysis. II. Non-associative models for sands', *Int. J. Numer. Analyt. Meth. Geomech.*, **9,** 477–498 (1985).
52. H. Hirai, 'An elastoplastic constitutive model for cyclic behaviour of sands', *Int. J. Numer. Analyt. Meth. Geomech.*, **11,** 503–520 (1987).
53. M. Pastor, O. C. Zienkiewicz and A. C. Chan, 'Theme/feature paper: Generalized Plasticity and the modelling of soil behavior', *Int. J. Numer. Analyt. Meth. Geomech.*, **14,** 151–190 (1990).
54. J. Ghaboussi and H. Momen, 'Modelling and analysis of cyclic behaviour of sand', in G. N. Pande and O. C. Zienkiewicz (eds), *Soil Mechanics-Transient and Cyclic Loads*, Wiley, New York, 1982, pp. 313–342.
55. H. B. Poorooshasb and S. Pietruszczak, 'On yielding and flow of sand; a generalized two-surface model', *Comput. Geotech.*, **1,** 33–58 (1985).

 © 1998 John Wiley & Sons, Ltd.

56. S. Pietruszczak and D. E. F. Stolle, 'Modelling of sand behaviour under earthquake excitation', *Int. J. Numer. Analyt. Meth. Geomech.*, **11,** 221–240 (1987).
57. O. A. Peku and V. Gocevski, 'Elasto-plastic model for cemented sand deposits', *Comput. Geotech.*, **7,** 155–187 (1989).
58. Z. Mroz and St. Pietruszczak, 'A constitutive model for sand with anisotropic hardening rule', *Int. J. Numer. Analyt. Meth. Geomech.*, **7,** 305–320 (1983).
59. J. H. Prevost, 'Plasticity theory for soil stress-strain behavior', *J. Engng. Mech. Div. ASCE*, **104,** 1177–1194 (1990).
60. J. H. Prevost, 'Two-surface versus multi-surface plasticity', *Int. J. Numer. Analyt. Meth. Geomech.*, **6,** 323–328 (1982).
61. S. Somasundaram and C. S. Desai, 'Modeling and testing for anisotropic behavior of soils', *J. Engng. Mech. ASCE*, **114,** 1473–1496 (1988).
62. G. W. Wathugala and C. S. Desai, 'Constitutive model for cyclic behavior of clays, I: theory', *J. Geotech. Eng. ASCE*, **119,** 714–729 (1993).
63. D. R. Katti and C. S. Desai, 'Modeling and testing of cohesive soil using disturbed-state concept', *J. Engng. Mech. ASCE*, **121,** 648–658 (1995).
64. D. Kolymbas (ed.), *Modern Approaches to Plasticity*, Elsevier, Amsterdam, 1992.

© 1998 John Wiley & Sons, Ltd.